CAPÍTULO 3

Remotely sensed biomass over steep slopes: an evaluation among successional stands of the Atlantic Rainforest, Brazil

CAPÍTULO 3

Remotely sensed biomass over steep slopes: an evaluation among successional stands of the Atlantic Rainforest, Brazil

Jomar Magalhães Barbosa[1]*, Ignacio Melendez-Pastor[2], Jose Navarro-Pedreño[2], Marisa Dantas Bitencourt[1]

[1] Department of Ecology, Institute of Biosciences, University of São Paulo, Brazil

[2] Department of Agrochemistry and Environment, University Miguel Hernández of Elche, Spain

Abstract

Ground forest biophysical data and remotely sensed images have been largely used to model and validate the biomass and carbon content on the landscape scale. Nevertheless, there is a lack of knowledge about modeling biomass using remotely sensed data from the steep slopes of the Atlantic Rainforest. In this context, the effect of topography on the biomass estimated from remotely sensed data was evaluated, and the modeled data was analyzed for different successional stands of the Atlantic Rainforest in southeastern Brazil. This modeling approach includes both satellite data (LANDSAT) and topographic features derived from a digital elevation model (TOPODATA). Our results yielded improved biomass estimates when modeling satellite data combined to a secondary geomorphometric variable (the illumination factor) based on hillshading (Adj. R^2 = 0.67 and RMSE = 35 Mg/ha). The modeled biomass yielded differing heterogeneity amongst the forest succession stages and indicated a higher frequency of elevated biomass values in areas with low illumination.

Keywords: aboveground biomass; forest succession; tropical forest, steep slope; remote sensing

1 – Introduction

Defining the spatial distribution of biomass in a forest enables the evaluation of how forested areas respond to human impact (Tangki and Chappell, 2008; Asner *et al.*, 2010) and environmental conditions (Saatchi *et al.*, 2007; Asner *et al.*, 2009). Moreover, the amount of forest biomass is important to the carbon cycle (IPCC, 2006; IPCC, 2010) because the rates of deforestation and forest regrowth determine the dynamics between carbon sources and sinks (Freedman *et al.*, 2009; Eckert *et al.*, 2011). In this context, estimates of the aboveground biomass (AGB), based on a

combination of field and remotely sensed data present an attractive tool for use on the landscape scale (Lu, 2006; Tangki and Chappell, 2008; Anaya *et al.*, 2009; Li *et al.*, 2010; Hall *et al.*, 2011; Hudak *et al.*, 2012). Despite increasing interest in AGB data, some forest types, such as the Brazilian Atlantic Rainforest (BARF), have few studies that model their biomass using remote sensing methods (Freitas *et al.*, 2005).

The BARF is one of the largest biodiversity centers in the world, and at the same time, this forest is threatened (Myers *et al.*, 2000; Dirzo e Raven, 2003). Different economic cycles (Dean, 1996) have led to an approximately 86% reduction in the forest area (approximately 129 million ha), according to SOS Mata Atlântica/INPE (2012). Some researchers have reported the regrowth of secondary forests in the BARF (Baptista & Rudel, 2006; Baptista, 2008; Lira *et al.*, 2012). Although these studies are both spatially and scale restricted, this tendency for regrowth has been explained by agricultural displacement from the BARF to the Amazon region (Pfaff and Walker, 2010; Walker, 2012).

The difficulty accessing steeply slope areas helped maintain the remaining Atlantic Rainforest in Brazil (Munroe *et al.*, 2007; Teixeira *et al.*, 2009), in addition to numerous other tropical mountain forests (Southworth and Tucker, 2001). Surveying the biomass in these mountainous regions is laborious, expensive and time consuming (Lu, 2006). Some success has been reported with estimating the AGB of steep-slope areas using remote sensing methods (Soenen *et al.*, 2010; Sun *et al.*, 2002; He *et al.*, 2012). However, the estimation error remains high due to the difficulty of minimizing satellite data distortion in areas with heterogeneous topography (Liu *et al.*, 2008). The combined difficulties of field surveys and satellite data processing in mountainous regions create the need to find alternative field survey strategies and new statistical approaches for modeling biomass (Soenen *et al.*, 2010).

This paper aims to map the AGB in different successional forest stands located in a region of rugged terrain. To that end, the specific objectives of this study are: 1) to evaluate the effect of topographical features on biomass estimates using remotely sensed data, and 2) to analyze the use of such estimates in the characterization of successional stands in the BARF. The topographic information was included during the modeling steps to analyze its influence on the biomass estimation. In addition, we compared the spatial pattern of the modeled biomass to the successional forest stands.

2 – Material and methods

2.1 - *Study area*

The study region is the largest remaining BARF of Brazil, which comprises 1,109,546 ha of continuous forests along the coastal mountains of São Paulo state (Ribeiro *et al.*, 2009). The field survey (24°33’ S and 48°39’ W; figure 1) was conducted in a topographically and biologically representative portion of the remaining forest. The field area encompassed approximately 15,000 ha within a topographically complex region with elevations ranging from 100 m to 900 m, and slopes ranging from 0° to 40° over a full range of terrain aspects. The climate is characterized by consistent rainfall throughout the year, with an annual rainfall of 2,000 mm and a mean annual temperature of over 21º C. The vegetation consists of ombrophilous tropical forests, which have approximately 100 to 160 species per hectare (Tabarelli and Mantovani, 1999) and a complex biophysical structure (Guilherme *et al.*, 2004; Marques *et al.*, 2009). Steep slopes within the study area reduced deforestation for intensive land use practices (Teixeira *et al.*, 2009). Historically, major forest disturbances occurred through the slash and burn agriculture system, which was practiced by small farmers

(Adams, 2000; Peroni and Hanazaki, 2002). This historical land use formed forest mosaics that include primary and secondary forests in different stages of regrowth.

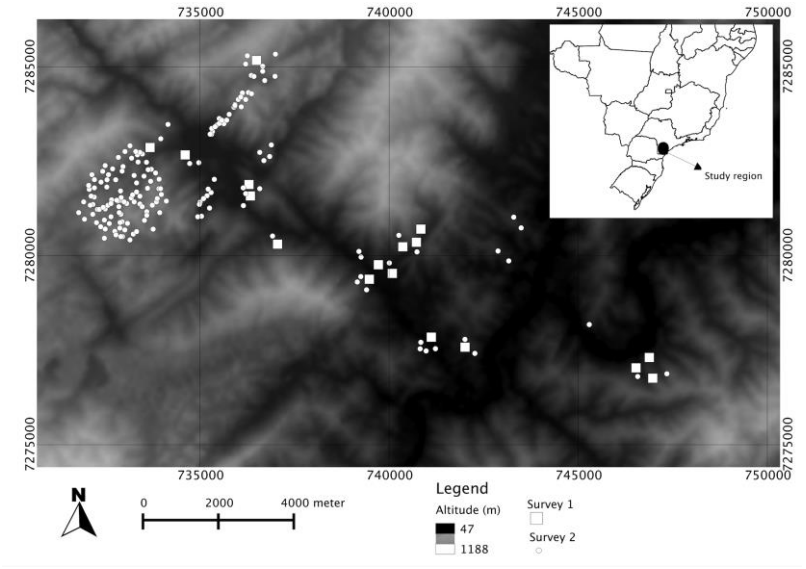

Figure 1. Digital elevation model of the surveyed area and the field data sampling (survey 1 and 2).

2.2 – *Vegetation field data*

Vegetation field data were collected in November, 2010 using a stratified sampling protocol that included three $IF_{hillshading}$ and two forest succession classes (see classifications on the topic 2.3). An initial survey (S1) of 170 points distributed across seventeen plots of 0.36 ha each were randomly distributed within the IF and forest classes to ensure an adequate representation of both the range of terrain and stand biomass. For each plot, 10 sample points, not overlapped, were randomly selected and surveyed via the point-centered quarter method (Cottam and Curtis, 1956). In the center of each sample point, four quadrants were divided, the nearest tree with a diameter at breast height (DBH) of over 4.9 cm in each quadrant was selected, and its total height, DBH and distance to the sample point were measured, totaling 40 trees for each plot (figure 2). Ten points sampled within a reduced area (0.36 ha) permitted sample trees

from sub-canopy, canopy and emergent. The distance and tree height measurements were taken with a laser distance meter (Leica DISTRO A5). The stand density at each plot (S) was calculated as follows:

$$S_i = 4 / (d_1^2 + d_2^2 + d_3^2 + d_4^2) \quad (1)$$

$$S = \Sigma S_i / n \quad (2)$$

where *Si* is the stand density of the ith sample point; d_1, d_2, d_3 and d_4 are the distances (m) from the central point to the nearest tree in each quadrant; n is the number of points; and S is the stand density with n points. The "S" value provides a relative area (m^2) among the surveyed trees, which is subsequently extrapolated to one hectare multiplying by 1 ha.

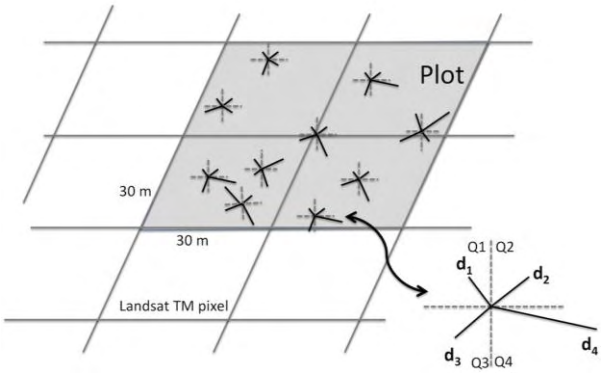

Figure 2: Sample design of the point-centered quarter method. Ten sampled points were scattered within the plot (Adapted from Main-Knorn *et al.*, 2011). Q_1, Q_2, Q_3, Q_4 are quadrants and d_1, d_2, d_3 and d_4 are the distances (m) of the central point to the nearest tree (DBH over 10 cm) in each quadrant.

A second sampling was taken for use in the model validation procedure and to ensure that the sample plot data were representative of the entire study area. For this second survey (S2), another 174 points scattered over the study area were measured using the same point-quadrant protocol. Subsequently, the modeled biomass and the

scattered points (S2) were statistically compared. The use of two complementary sample protocols ensured the total characterization of the vegetation and minimized the difficulty accessing the studied area, which was characterized by an absence of roads and intricate forest structures.

The AGB of the sampled trees was calculated using an allometric equation derived from a destructive method used in patches of the BARF (Eq. 3). This equation was obtained from dry biomass from tree leaves, branches and trunks (Burger and Delitti, 2008) and was used due to the structural similarity between our study area and that used by the authors:

$$Ln(AGB_i) = -3.676 + 0.951 \times Ln(DBH^2 \times h) \quad (3)$$

where AGB_i is the dry aboveground biomass (kg) of the tree, DBH is the diameter at breast height (cm), and h is the total tree height (m). The stand tree density was multiplied by the mean AGB of each plot sampled. We choose this allometric equation because those elaborated from the Amazon overestimate the biomass of Brazilian Atlantic Forests by approximately 24–30% (Alves *et al.*, 2010). These differences are expected because the mean tree height of an Amazonian forest is greater than that of an Atlantic forest with a similar DBH (Vieira *et al.*, 2008). A general biomass-carbon conversion factor of 47.4% (±2.51% S.D.) was used despite generic conversion factors lead to overestimates because the stem wood C content is highly variable among co-occurring tropical tree species (Martin and Thomas, 2011).

2.3 –*Topographic and image data processing*

The terrain data for the topographic correction of the satellite images and biomass modeling were acquired using a digital elevation model (DEM). The DEM was obtained from TOPODATA (http:// www.dsr.inpe.br/topodata), a Brazilian geomorphometric database (Valeriano *et al.*, 2006; Valeriano, 2008). TOPODATA is

available for the entirety of Brazil and has been refined to 1 arc-sec (~ 30 m) resolution through an interpolation process using the Shuttle Radar Topography Mission (Valeriano and Albuquerque, 2010, Valeriano and Rossetti, 2012). Resampling the DEMs with geostatistical approaches, such as on the TOPODATA, produces a satisfactory final result even though it does not increase the level of detail (Grohmann and Steiner, 2008; Mantelli *et al.*, 2011). Instead, this technique preserves the coherence of the angular properties (i.e., slope and aspect) of neighboring pixels (Valeriano *et al.*, 2006) and can be an important source of data in regions where original 1'' DEM is unavailable. The DEM and both the solar azimuth (84.89°) and zenith (27.37°) acquired at the same time as the Landsat TM data were used to obtain the illumination factor (IF), which is a relief enhancement used to evaluate the solar illumination pattern (Canavesi, 2008; Valeriano and Albuquerque, 2010; Valeriano, 2011). The IF was used in the present study as an explanatory variable on the modeling biomass.

Using spherical trigonometry, we calculated the IF in three separate ways: {1}using a hillshade variable scaled between 0 and 2 (considering the direction of the ground, slope, solar azimuth, and solar zenith (Eq. 4) (Canavesi, 2008), {2} using a sum of orthogonal vectors (Eq. 5) (Canavesi, 2007; Valeriano and Albuquerque, 2010), and {3} using the law of cosines (Eq. 6) (Slater, 1980; Valeriano, 2011):

$$IF_{hillshading} = \sqrt{(\cos(\varphi_{x,y} - \varphi_s) + \cos(\theta_{x,y} - \theta_s))^2} \quad (4)$$

$$IF_{vector\ sum} = \sqrt{(\cos(\varphi_{x,y} - \varphi_s))^2 + (\cos(\theta_{x,y} - \theta_s))^2} \quad (5)$$

$$IF_{cosi} = \cos\theta_{x,y}\cos\theta_s + \sin\theta_{x,y}\sin\theta_s\cos(\varphi_s - \varphi_{x,y}) \quad (6)$$

where: IF = the illumination factor (scaled from 0 to 2), $\varphi_{x,y}$ = aspect, φ_s= solar azimuth, $\theta_{x,y}$ = slope, and θ_s = solar zenith. The last four variables are expressed in degrees.

In addition to the topographical data, Landsat Thematic Mapper (TM) satellite imagery was also used as an explanatory variable in the biomass estimation. These data were acquired November 19, 2010 (path 220 and row 77), which is the same period of the field survey. First, the level-1 TM data were converted from digital numbers to a spectral radiance using published calibration gain and offset values (Chander *et al.*, 2010). The image bands were then converted to top of atmosphere reflectance and atmospherically corrected based on the COS-T1 model, which considers the earth-sun distance, mean exoatmospheric solar irradiance, solar zenith angle and dark object subtraction (Chavez, 1996; Lu *et al.*, 2002). The topographic correction of the TM images was processed using C and SCS+C corrections (these equations can be found in Soenen *et al.*, 2005). The SCS+C corrections are based on the photometric Sun-Canopy-Sensor method and theoretically preserve geotropic nature of the vertical tree growth and best performing the C-correction (Soenen *et al.*, 2005; Soenen *et al.*, 2010).

The biomass was estimated using separate TM bands and with vegetation indices, such as the normalized difference vegetation index (NDVI) and enhanced vegetation index (EVI). The NDVI was calculated as (near infrared−red) ÷ (near infrared +red) and the EVI was calculated as (near infrared −red) ÷ (near infrared +6×red−7.5×blue+1) (Huete *et al.*, 1997).

The TM data were also used to elaborate a land cover classification focusing on successional forest stands. We processed the KMEANS algorithm using all of TM bands in an unsupervised classification. Six land cover classes were identified: the initial secondary forest, the advanced secondary forest/Primary forest, urban, settlements (productive fields, pasture) and abandoned anthropic settlements (Table 1). Advanced secondary forest and primary forest stands were grouped into the same class due to errors during spectral mixing. The map accuracy was assessed using a 200 point

validation dataset by computing the Kappa coefficient (Pontius, 2000). This land cover validation dataset encompassed 100 field-georeferenced ground truth points and another 100 points obtained from ALOS imaging (date 2010 and 10 meters spatial resolution) and SPOT images from Google Earth® (date 2010). Image-based validation points were used to evaluate the classification error of inaccessible field locations.

Table 1: Description of the land cover classes.

Land cover classes	**Description of each class**
Water	Rivers and small ponds
Anthropic settlement	Agricultural, pastures
Urban	Cities and small villages
Abandoned anthropic settlement	Abandoned agricultural or pasture areas
Initial secondary forest	Forested area (highest trees less than 10 m tall)
Advanced secondary forest / Primary forest	Forested area (highest trees over 10 m tall)

2.4 – *Predictive biomass modeling*

The biomass model was developed by linking the field AGB data from the sample plots (S1) to the Landsat TM and DEM data using the generalized linear model (GLM). The GLM is commonly used in environmental research (Guisan and Zimmermann, 2000) and has been increasingly popular in remote sensing (Schwarz and Zimmermann, 2005; Mathys *et al.*, 2009; Kajisa *et al.*, 2009) because it allows for non-linear and non-constant variance structures in the data (Bolker, 2008). For a comprehensive description of the GLM, refer to McCullagh and Nelder (1989). All of the modeling steps were implemented using the statistical R Development Core Team, 2011, version 2.0.0.

The biomass was estimated using a set of input data, such as the Landsat

reflectance (TM1, TM2, TM3, TM4, TM7 bands), NDVI, and EVI, and topographic data, such as IF, slope, and aspect (Figure 3). The Landsat data were analyzed considering both the corrected and uncorrected topographic images. The modeling was processed by linking the averages of the spatially coinciding satellite data for each plot sampled in the S1 field survey. To avoid multicollinearity amongst the explanatory variables, the variation inflation factor (VIF) and tolerance (O' Brien, 2007) were used to define any correlations. The VIF and tolerance were calculated from equations 7 and 8, respectively:

$$VIF = 1 / 1 - R^2 \quad (7)$$

$$Tolerance = 1 / VIF \quad (8)$$

In addition, the explanatory variables were either included or excluded from the GLMs using Akaike's Information Criterion (AIC) (Akaike, 1974) and calculating their significance. The model plausibility was evaluated using the R-squared, ΔAICc and Akaike weights. ΔAIC values less than or equal to 2 indicate that the model best fit the observed data, and the Akaike weights indicate the probability that the model was the best of the candidate models (McCullagh and Nelder, 1989).

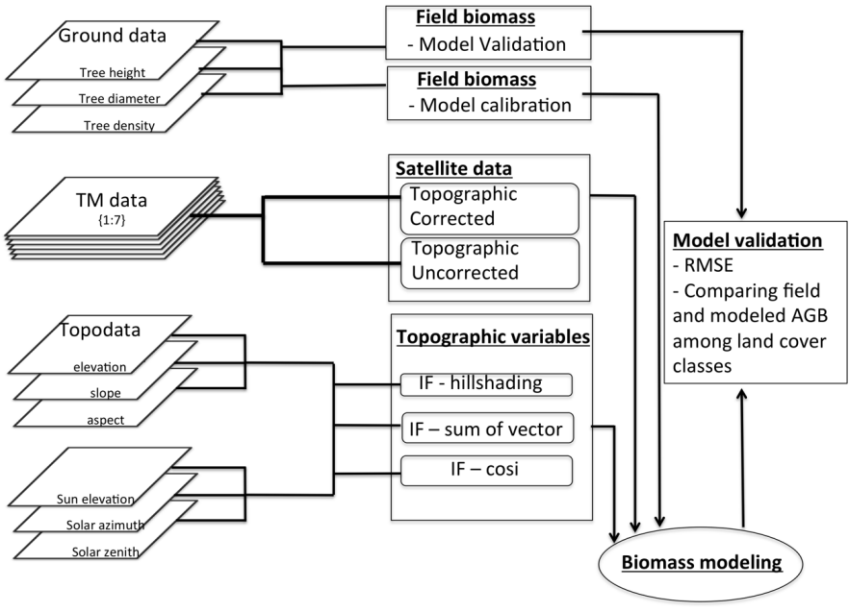

Figure 3: Procedure for predicting biomass from TM, inventory plot and topographic data.

2.5 – *Estimated AGB versus field data*

The estimation error was calculated using the root mean square error (RMSE) between the field and modeled data. In this validation procedure, we randomly selected 70% of the total data sets from 17 plots one hundred times. For each selection, we obtained the RMSE between the remaining 30% field biomass values and the model estimates. Next, we evaluated the reliability of each model using the mean of the 100 RMSE values. Finally, we analyzed the bias trends of the models from the percent error for 1,000 comparisons between the observed and predicted data. These comparisons allowed any positive or negative trends in the errors to be detected.

To ensure that the biomass estimated using the plot data was representative of the entire study area, we compared the modeled data with the S2 samples. First, we obtained the average modeled AGB for 20 polygons (0.81 ha each) randomly distributed over each forest class and compared to the field biomass from S2. Both the field and modeled biomass were statistically compared for each forest class using their

means and standard deviations. We assumed that the highest similarity between the field and modeled data represents the highest feasibility of the modeled biomass. Finally, we investigated the relationship between the predicted biomass and the best-performed explanatory variable from 78 new points randomly scattered in the studied region.

3 – Results

3.1 – *Field forest structure*

The forest stand parameters corresponding to the 344 surveyed points are shown in Table 2. The average AGB in the studied area was 107 Mg/ha. There were 227 (66%) sampled points in the advanced successional stand, with mean biomass of 128 Mg/ha, and 117 points (34%) in the initial forest stand, with mean biomass of 54 Mg/ha. The low global mean AGB is due the inclusion in the sample of different forest successional stands. The high standard deviation of the mean biomasses (Table 2) indicates the large range of biomass values surveyed for each biomass class. This large forest structure variation within the sampled data ensured that different forest succession stages were included in the modeling procedure.

Table 2: Summary of the mean (standard deviation) forest stand parameters for each forest successional class.

Successional stage	Tree diameter (cm)	Tree height (m)	Tree density (ind./ha)	Biomass (Mg/ha)
Initial	10 (4)	7 (2)	2084 (1927)	54 (68)
Advanced	14 (5)	9 (2)	2185 (1306)	128 (190)
Total	13 (5)	8 (2)	2144 (1491)	107 (170)

3.2 – Topographic patterns

The mountainous pattern of the studied area forms a complex mosaic of areas with different illumination factors. The IF_{cosi} and $IF_{hillshading}$ had higher values when the

related slope aspect was similar to the sun azimuth (84.89°) at the time of the Landsat TM acquisition used in this study (Figure 4). However, the $IF_{vector\ sum}$ possessed two peaks of high IF relating to the slope aspect.

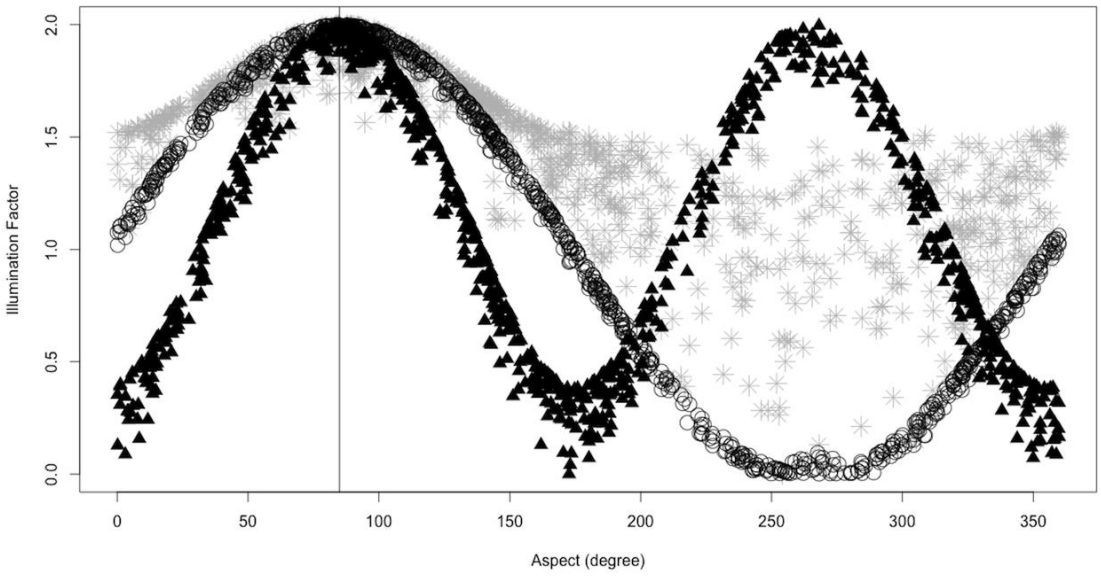

Figure 4: Illumination factors in a horizontal direction with a longitude of 48.80° (W). The triangle plots are the $IF_{vector\ sum}$, the asterisks are the IF_{cosi} and circles are the $IF_{hillshading}$. The values from the $IF_{vector\ sum}$ and IF_{cosi} were rescaled to 0 to 2 to compare to the results of the $IF_{hillshading}$. The vertical line represents the sun azimuth from the same time of the TM data acquisition (84.89°).

3.3 – *Modeling biomass using both field and remote sensed data*

The AIC approach to model selection only identified one model as a plausible predictor of forest AGB ($\Delta AIC_c < 2$). Table 3 summarizes the six best models relative to the null model. The explanatory variables, such as the slope, aspect, NDVI, and EVI were not showed due to their poor predictions. The model that combined the topographically uncorrected Landsat TM5 (1.55 – 1.75 μm) and IFhillshading was the most predictive of the AGB (R^2 = 0.67; RMSE = 35 Mg/ha). This model had a reduced probability of finding large errors (Figure 5a) and showed two error peaks of approximately 25% for both the negative and positive tendencies (Figure 5b). The

relationship between the predicted and observed AGB for this model is shown in the Figure 6. The multicollinearity test for model 1 indicates a VIF of 2.9 and tolerance of 0.34.

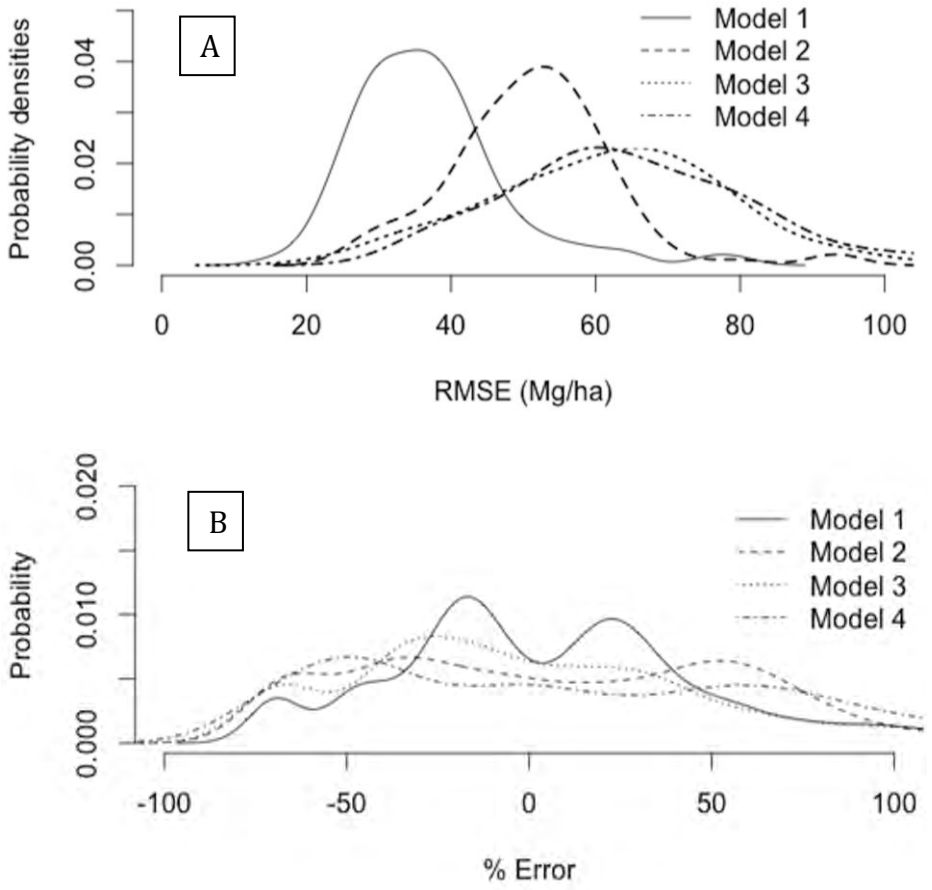

Figure 5: Histogram of the probability densities of the best four models for (a) the randomized RMSE and (b) for biases tendency using the error percentage. The model numbers are the same for both figures as in Table 3. The histograms were normalized.

Table 3: Summary of the suitability of the models. ΔAIC_c = Akaike Information Criterion, Adj. R^2 = Adjusted coefficient of determination, RMSE = root mean square error, AGB = aboveground biomass, TM5 = mid-infrared Landsat TM, IF = Illumination Factor. The models used the identity link-function.

Model	**Fitting parameters**				**Values**			
	ΔAIC_c	**Weight**	**Adj. R^2**	**RMSE (Mg/ha)**	**Variable name**	**Estimate (β)**	**Std. Err. (β)**	**ρ-Level**
Model 1	0.0	0.95	0.67	35	Intercept	-6.04644	1.83352	0.0050
					Ln(TM5)	-5.44825	0.95790	0.0001
					Ln(TM5) × Ln($IF_{hillshading}$)	-0.22188	0.05939	0.0022
Model 2	6.5	0.036	0.52	52	Intercept	-1.1382	1.3758	0.4219
					Ln(TM5)	-3.0333	0.7122	0.0007
					Ln(TM5) × Ln($IF_{vectorsum}$)	1.2074	0.5378	0.0414
Model 3	7.9	0.017	0.40	60	Intercept	-7.736	3.575	0.0470
					Ln(TM5 SCS-C correction)	-6.143	1.801	0.0038
Model 4	9.0	0.010	0.44	63	Intercept	-0.464	1.45999	0.7553
					Ln(TM5)	-1.684	0.90784	0.0848
					Ln(slope) × Ln(aspect)	0.096	0.06098	0.1353
Model 5	10.2	0.005	0.39	62	Intercept	-4.5288	3.7172	0.2432
					Ln(TM5)	-4.7679	2.0757	0.0376
					Ln(TM5) × Ln(IF_{cosi})	-0.9651	0.8388	0.2692
Model 6	11.8	0.002	0.24	59	Intercept	-6.116	4.227	0.1685
					Ln(TM5 C correction)	-5.579	2.231	0.0245
Null model	14.7	<0.001						

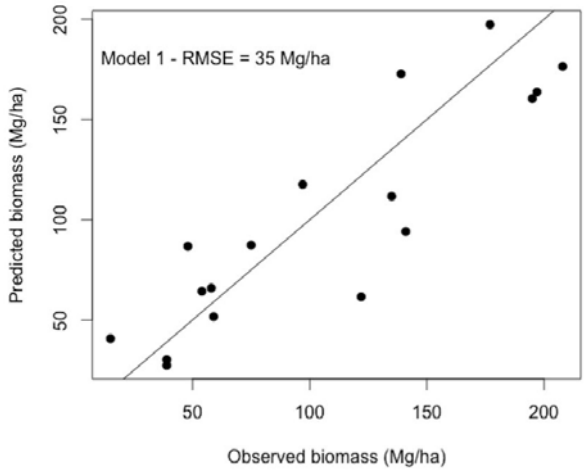

Figure 6: Relationship between observed biomass and that predicted by the GLM defined in the model 1 [Ln(AGB) = -6 – 5.4(Ln(TM5)) – 0.2(Ln(TM5) x Ln($IF_{hillshading}$))].

The biomass model for the initial and advanced/primary forest classes developed using model 1 demonstrated different visual patterns (Figure 7). Furthermore, the estimated biomasses using 20 pixel windows (3 × 3 pixels) randomly scattered in each of the forest succession classes were 50.3 Mg/ha (SD = 17 Mg/ha) for the initial secondary forest and 172.7 Mg/ha (SD = 66 Mg/ha) for the advanced secondary forest/primary forest classes. These modeled data were closely related to the scattered field survey points (S2) with a mean field biomass of 54 Mg/ha (SD = 68 Mg/ha) for the initial secondary forest and 128 Mg/ha (SD = 190

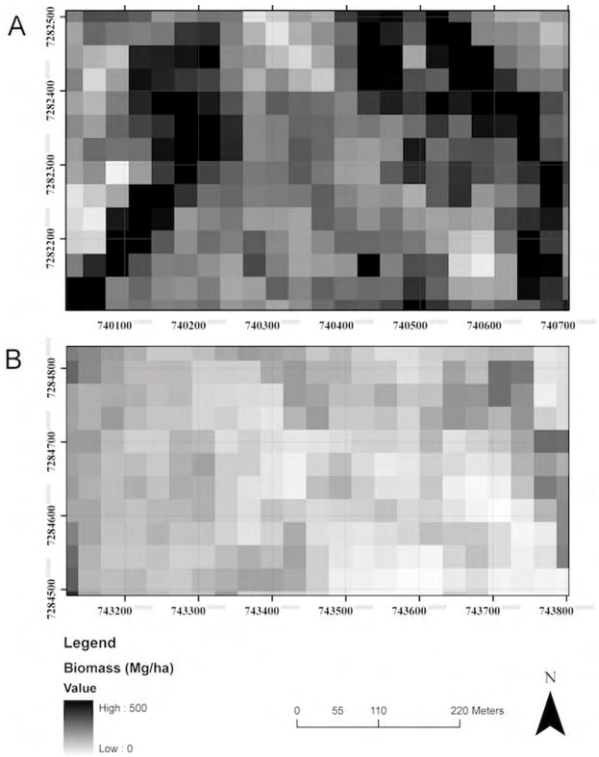

Figure 7: Biomass maps over two forest areas elaborated using the best model (model 1). (A) Advanced secondary forest/primary forest and (B) initial secondary forest.

Mg/ha) for the advanced secondary forest/primary forest classes (Figure 8). There were no statistical differences between these field-based data and the modeled data ($\rho < 0.05$). While the estimated biomass of the initial forest succession class possessed low heterogeneity, the advanced forest class showed high variance in the modeled biomass of randomly selected plots (Figure 9). The advanced forest succession class possessed higher differences for the modeled biomass both between the plots and within each plot.

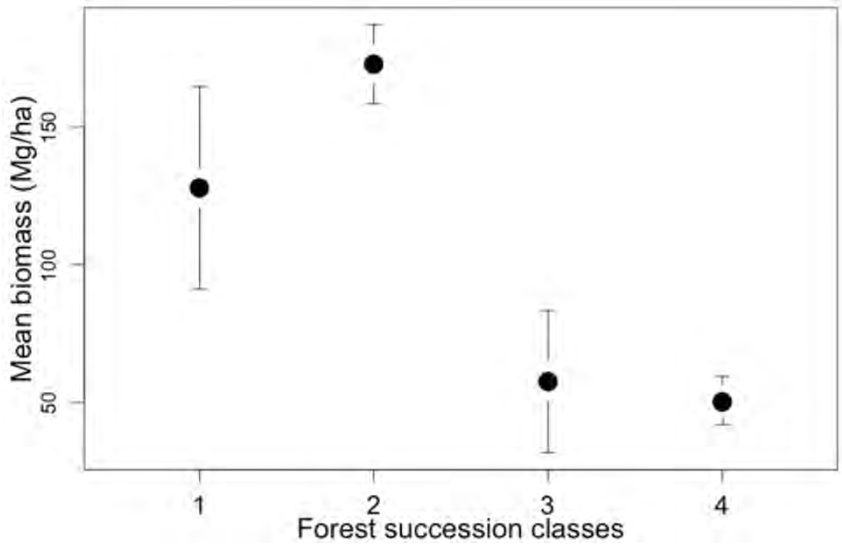

Figure 8: Mean biomass and confidence intervals (95%). 1: Field biomass in the advanced forest class. 2: Modeled biomass in the advanced forest class. 3: Field biomass in the initial forest class. 4: Modeled biomass in the initial forest class.

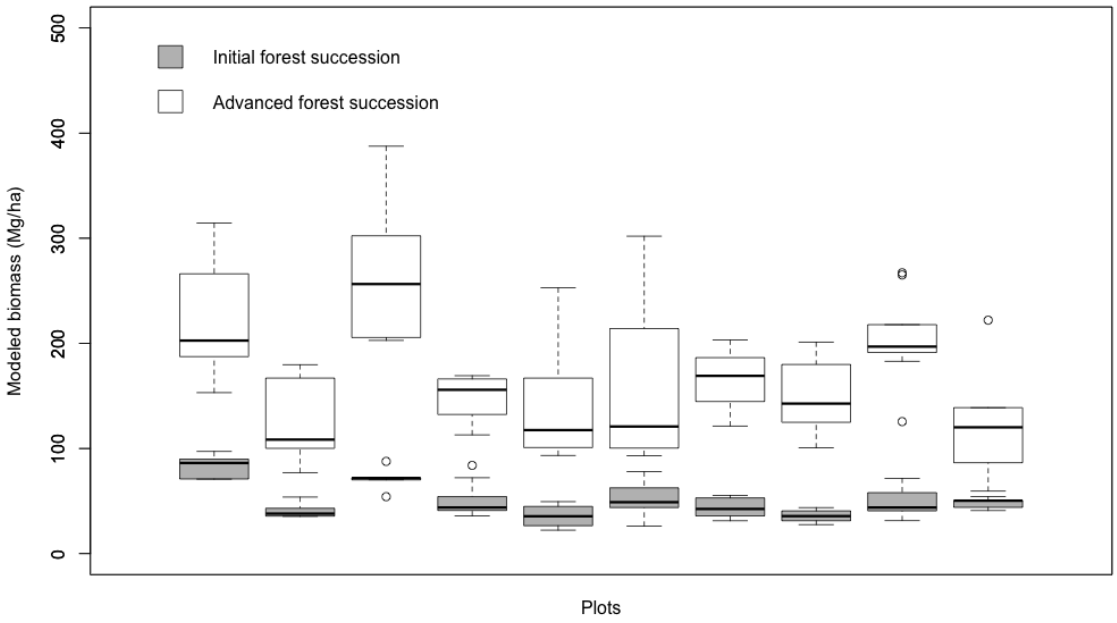

Figure 9: Boxplot of the mean modeled biomass over 20 plots (0.81 ha each) randomly scattered throughout the landscape and comprising both the initial and advanced forest succession classes.

The land-cover map (Figure 10) yielded an overall kappa of 0.80 (Congalton, 1991). Although the accuracy was acceptable, the error matrix merges the initial secondary forests with abandoned anthropic settlements. As illustrated in Table 4, the studied region has a large forested area (76.4% of the total area). The sum of all anthropic settlements represents 22.75% of the studied area (pasture, subsistence agriculture, urban, and abandoned settlements). The best biomass model indicates approximately 23.8 (±1.25) TC/ha and 81.8 (±4.33) TC/ha for the initial secondary forest and advanced secondary/primary forest classes, respectively. Considering the forested area of each land cover class, the studied landscape (Fig. 10) stored approximately 5 million T of aboveground carbon. We found a negative, though weak, relation between the modeled biomass and the IFhillshading value ($r = -0.32$; $\rho = 0.004$), which indicates a tendency for elevated biomass values in areas with low illumination factors (Figure 11).

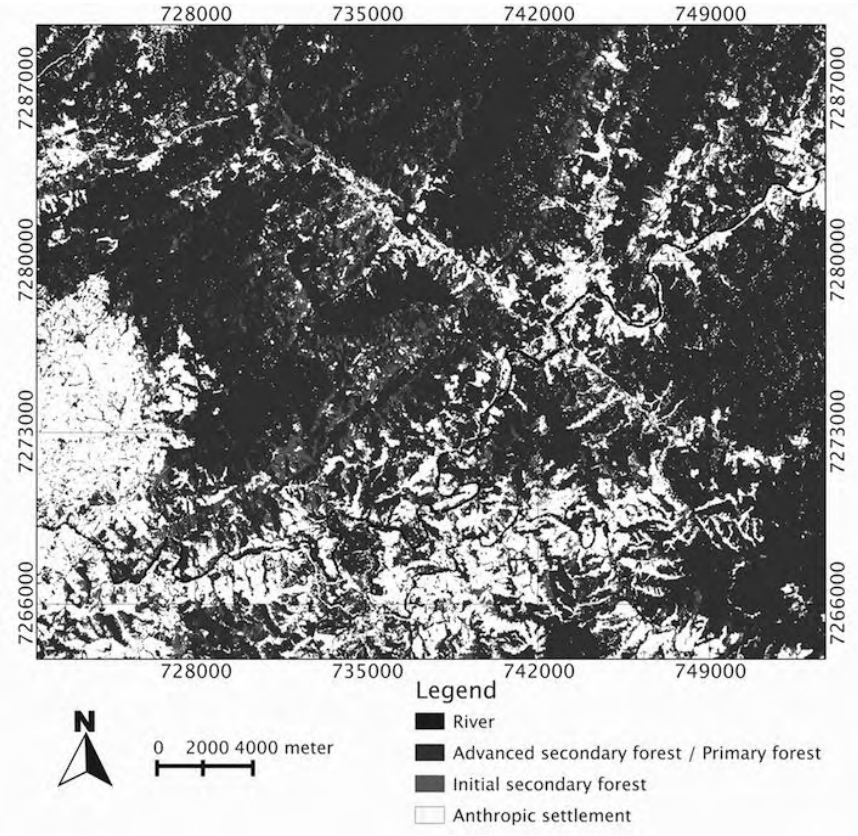

Figure 10: Land-cover map of the studied area.

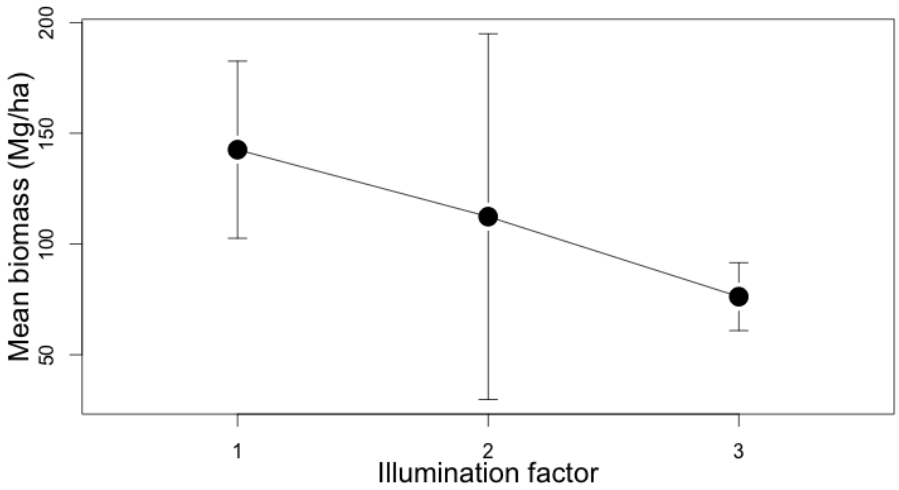

Figure 11. Mean modeled biomass and confidence intervals (95%) 1 - Illumination factor from 0 to 0.66; 2 - Illumination factor from 0.66 to 1.33; and 3 - Illumination factor from 1.33 to 2.

4 – Discussion

The integration between both the point-centered quarter method and the plot-based approach for surveying forest structure shows similar results for studies limited to plot-based survey of the BARF (Alves *et al.*, 2010; Borgo, 2010). This sample protocol allowed the survey of plots with large area (i.e. 0.36 ha) with a reduced number of field workers to sample a higher number of locations throughout the landscape. The use of large plots permits a more representative inclusion of the biophysical variation of the vegetation in the sample and results in minors model inaccuracies due to GPS positional errors (Frazer *et al.*, 2011; Zolkos *et al.*, 2013). However, the point-centered quarter method estimates, instead measure, tree density. Moreover, sampling a reduced number of points within forest stands with trees distributed aggregately generates estimative errors when compared with fixed-area plots that measure all trees (Bryant *et al.*, 2004). Although these possible source of error, we assumed that the biophysical forest stand within only 0.36 ha present weak deviates from a random spatial pattern and that ten points (measuring 40 trees) may produce reliable forest structure estimates of this reduced area. Landsat TM5 imaging used with a secondary geomorphometric variable (the IF), based on the hillshading characteristic, provided advanced biomass predictions for the studied Atlantic Rainforest area. The results yielded poor biomass estimates when the model used topographically corrected images. Alternatively, using topographic data as an explanatory variable produced biomass estimates with a reduced prediction error. The correlation between the biomass and terrain variables was significant (Fig. 11), as shown by previous studies (Sun *et al.*, 2002; He *et al.*, 2012; Dahlin *et al.*, 2012). Therefore, both the explicit parameterization of the sun reflection geometry and the inclusion of topographic data in the model are alternatives to increment these predictions (Soenen *et al.*, 2010; Main-Knorn *et al.*, 2011). To this end,

the present study provided a new parameterization of the topography data as a single variable for modeling biomass.

The $IF_{hillshading}$ showed better performance for estimating the biomass than both $IF_{vectorsum}$ and IF_{cosi}. These three IF values relate differently to the aspect data (Fig. 4), indicating that each highlights a different terrain pattern. The $IF_{hillshading}$ separates the sunlight directly incident and opposite to the surface. These data constitute the relief enhancement from the effect of solar illumination on the satellite data (Canavesi, 2008; Valeriano and Albuquerque, 2010; Valeriano, 2011), and their inclusion on the modeling increased the performance of the biomass estimates. Although our experimental approach did not focus on explaining the sunlight effect has on the forest biomass, we found higher frequency of elevated biomass in areas with a low illumination factor. These tendencies are probably related to the maintenance of an elevated biomass (advanced forest succession and primary forests) in shaded and isolated areas that experienced less historical agriculture usage (Munroe *et al.*, 2007; Silva *et al.*, 2008; Teixeira *et al.*, 2009).

Topographic corrections, such as the C-correction and Minnaert corrections, appear to be capable of reducing the topographic effects to a certain degree, but only for highly non-Lambertian surfaces (Wu *et al.*, 2008). More recent approaches, such as the SCS+C (Soenen *et al.*, 2005), are more concise and compensate for changes in the self-shadowed area across the range of canopy complexities (Kane *et al.*, 2008). However, our results suggest that topographic corrections do not perform well with our datasets, which is possibly because of the intricate orography and complexity of the forest stands. The topographic correction of the satellite images was based on the assumption that there was a linear relationship between the sun reflectance and the cosine of the angle between the normal of the ground and the solar beam (Ekstrand, 1996). Nevertheless,

the scatterplot of both variables failed to generate a suitable linear regression. For this reason, using the IF on the modeling biomass of our study area significantly improves the model estimates relative to topographically corrected images.

Most recent remote sensing biomass estimates of tropical forests employ active systems such as RADAR or LIDAR (Englhart *et al.*, 2011; Saatchi *et al.*, 2011), while others employ passive optical systems (Tangki and Chappell, 2008; Kajisa *et al.*, 2009; Li *et al.*, 2010; Wijaya *et al.*, 2010; Sarker and Nichol, 2011) or a combination of both (Bitencourt *et al.*, 2007; Wang and Qi, 2008; Cutler *et al.*, 2012). Although cloud coverage in tropical regions and satellite data saturation are major constraints for passive optical systems when modeling tropical forest biomass (Lu, 2006), the increased accessibility of many existing passive optical systems compared to other technologies and the availability of historical images (i.e., Landsat program) provides a large pool of data suitable for biomass mapping. Moreover, the lower biomass amount in BARF than in Amazon (Vieira *et al.*, 2008; Anderson, 2012) may reduce saturation effect in our biomass model. Previous studies of Brazilian tropical forests found that using mid-infrared spectral bands for biomass estimates minimized the pixel saturation (Steininger, 2000; Freitas *et al.*, 2005). Our results agree with this statement, as demonstrated by the inclusion of the mid-infrared Landsat band (TM5) in better performing models.

Both the field and modeled biomass data showed similar mean values for both the initial and advanced forest classes (Fig. 9). These results indicate the feasibility of predicting the AGB for different forest succession stages. The modeled biomass permitted the evaluation of the structural heterogeneity inside the forest class (Fig. 10). This finding indicates that spatially explicit AGB estimates can provide qualitative information about the forest successional stage and may be used to investigate forest regrowth when an increase in the forest area does not exist. Different authors have

studied the forest succession using historical analysis or stand classes (Neeff *et al.*, 2006; Liu *et al.*, 2008; Helmer *et al.*, 2009; Sirén and Brondizio, 2009). However, forest age classes and stages (i.e., initial, intermediate and advanced) were not equally defined by these authors. The lack of standardization in successional stands may be a problem when comparing different studies. The species composition and forest structure such as biomass, diameter and height, can be better suited to defining the successional stage (Vieira *et al.*, 2003).

In Brazil, many remote sensing studies have been conducted in the Amazon (Foody *et al.*, 2003; Lu *et al.*, 2004; Li *et al.*, 2010; d'Oliveira *et al.*, 2012), which has resulted in Amazon-based biomass estimates being used at the national level due to the minimal effort to measure the AGB of other biomes such as the BARF. Biomass estimates in the BARF have had previously studied with field-based studies (Vieira *et al.*, 2008). Few studies have measured the large-scale biomass in the BARF using remote sensing data. In this context, the present study provides important tools for inferring the biomass on steep slopes in the Atlantic Rainforest.

5 – Conclusions

This study provides a feasible framework for estimating the aboveground forest biomass in the Atlantic Rainforest with reduced field requirements. In addition, the results indicate that a secondary geomorphometric variable with different topographic data to form a unique dataset significantly improved the biomass estimates in a mountainous area. The reduced time required to calibrate the model when using the point quadrant method can provide an alternative survey strategy to estimate the field biomass and promote the validation of biomass maps. However, this methodology can be better evaluated using other forest types and different optical satellite data. Considering the scarcity of remotely sensed biomass data from the Atlantic Rainforest,

our results present an important source of information about large-scale biomass estimation in this biome and demonstrate that the forests remaining distributed on the steep slopes in the BARF form important carbon pools.

Acknowledgment

Coordenação de Aperfeiçoamento de Pessoal de Nível Superior (CAPES) for the scholarship.

6 - References

Adams, C., 2000. As roças e o manejo da Mata Atlântica pelos caiçaras: uma revisão. Interciência 25 (3), 143-150.

Anderson, L.O., 2012. Biome-Scale Forest Properties in Amazonia Based on Field and Satellite Observations. Remote Sensing 4 (5), 1245-1271.

Akaike H (1974) A new look at the statistical model identification. IEEE Trans Automat Contr 19 (6),716–723.

Alves, L.F., Vieira, S.A., Scaranello, M.A., Camargo, P.B., Santos, F.A.M., Joly, C.A., Martinelli, L.A., 2010. Forest structure and live aboveground biomass variation along an elevational gradient of tropical Atlantic moist forest (Brazil). Forest Ecology and Management 260 (5), 679-691.

Anaya, J. A., Chuvieco, E., & Palacios-Orueta, A., 2009. Aboveground biomass assessment in Colombia: A remote sensing approach. Forest Ecology and Management 257 (4), 1237-1246.

Asner, G.P., Hughes, R.F., Varga, T.A., Knapp, D.E., Kennedy-Bowdoin, T., 2009. Environmental and Biotic Controls over Aboveground Biomass Throughout a Tropical Rain Forest. Ecosystems 12 (2), 261-278.

Asner, G.P., Martin, R. E., Knapp, D. E., Kennedy-Bowdoin, T., 2010. Effects of Morella faya tree invasion on aboveground carbon storage in Hawaii. Biol. Invasions 12, 477–494. DOI 10.1007/s10530-009-9452-1

Baptista, S. R., 2008. Metropolitanization and forest recovery in southern Brazil: a multiscale analysis of the Florianópolis city-region, Santa Catarina State, 1970 to 2005. Ecology and Society, 13 (2), 5.

Baptista, S.R., & Rudel, T.K., 2006. A re-emerging Atlantic forest? Urbanization, industrialization and the forest transition in Santa Catarina, southern Brazil. Environmental Conservation 33 (3), 195-202.

Bitencourt, M.D., de Mesquita Jr., H.N., Kuntschik, G., 2007. Cerrado vegetation study using optical and radar remote sensing: two Brazilian case studies. Can. J. Remote Sensing 33 (6), 468-480.

Bolker, B. M., 2008. Ecological models and data in R. New Jersey: Princeton University Press. 396p.

Borgo, M., 2010. A Floresta Atlântica do litoral norte do Paraná, Brasil: aspectos florísticos, estruturais e estoque de biomassa ao longo do processo sucessional. PhD in Forestry, Paraná Federal University, Curitiba, Brazil, 165 pp. < http://www.floresta.ufpr.br/pos-graduacao/defesas/pdf_dr/2010/t283_0319-D.pdf> (Accessed 25 July 2012).

Bryant, D.M. *et al.*, 2004. Forest community analysis and the point-centered quarter method. Plant Ecology 175 (2), 193-203.

Burger, D.M.D., Deletti, W.B.C., 2008. Allometric models for estimating the phytomass of a secondary Atlantic Forest area of southeastern Brazil. Biota Neotropica 8 (4), 131-136.

Canavesi, V., 2008. Aplicação de dados Hyperion EO-1 no estudo de plantações de Eucalyptus spp. In, PhD in the Remote Sensing Department, Instituto Nacional de Pesquisas Espaciais (INPE). São José dos Campos, SP, INPE. < http://mtc-m18.sid.inpe.br/col/sid.inpe.br/mtc-m18@80/2008/08.07.14.39/doc/@4primeirasPaginas2008-08-07-12-29-36.pdf> (Accessed 15 January 2011).

Canavesi, V., Ponzoni, F.J., 2007. Relações entre variáveis dendrométricas de plantios de Eucalyptus sp. e valores de FRB de superfície de imagens do sensor TM/Landsat 5. In: INPE (Ed.), XIII Simpósio Brasileiro de Sensoriamento Remoto (pp. 1619-1625). Florianópolis, Brasil: Instituto de Pesquisas Espaciais (INPE).

Chander, G., Haque, M.O., Micijevic, E. and Barsi, J.A., 2010. A Procedure for Radiometric Recalibration of Landsat 5 TM Reflective-Band Data. IEEE Transactions on Geoscience and Remote Sensing 48 (1), 556-574.

Chavez, P.S., 1996. Image-based atmospheric corrections revisited and improved. Photogrammetric Engineering and Remote Sensing 62 (9), 1025-1036.

Congalton, R.G., 1991. A review of assessing the accuracy of classifications of remotely sensed data. Remote Sensing of Environment 37 (1), 35-46.

Cottam, G., Curtis, J. T., 1956. The Use of Distance Measures in Phytosociological Sampling. Ecology 37 (3), 451-460.

Cutler, M.E.J., Boyd, D.S., Foody, G.M., Vetrivel, A., 2012. Estimating tropical forest biomass with a combination of SAR image texture and Landsat TM data: An assessment of predictions between regions. ISPRS Journal of Photogrammetry and Remote Sensing 70, 66–77. http://dx.doi.org/10.1016/j.bbr.2011.03.031

Dahlin, K.M., Asner, G.P. and Field, C.B., 2012. Environmental filtering and land-use history drive patterns in biomass accumulation in a mediterranean-type landscape. Ecological Applications 22 (1), 104-118.

Dean, W., 1996. A Ferro e Fogo: a História da Devastação da Mata Atlântica. São Paulo: Companhia das Letras. 484p.

Dirzo, R. and Raven, P.H., 2003. Global state of biodiversity and loss. Annual Review of Environment and Resources, 28: 137-167. doi:10.1146/annurev.energy.28.050302.105532

d'Oliveira, M.V.N., Reutebuch, S.E., McGaughey, R.J., Andersen, H.-E., 2012. Estimating forest biomass and identifying low-intensity logging areas using airborne scanning lidar in Antimary State Forest, Acre State, Western Brazilian Amazon. Remote Sensing of Environment 124, 479-491. doi:10.1016/j.rse.2012.05.014

Eckert, S., Ratsimba, H. R., Rakotondrasoa, L. O., Rajoelison, L. G., & Ehrensperger, A., 2011. Deforestation and forest degradation monitoring and assessment of biomass and carbon stock of lowland rainforest in the Analanjirofo region, Madagascar. Forest Ecology and Management 262 (11), 1996-2007.

Ekstrand, S., 1996. Landsat TM-Based Forest Damage Assessment: Correction for Topographic Effects. Photogrammetric Engineering & Remote Sensing 62 (2), 151-161.

Englhart, S., Keuck, V., Siegert, F., 2011. Aboveground biomass retrieval in tropical forests—The potential of combined X- and L-band SAR data use. Remote Sensing of Environment 115 (5), 1260–1271.

Frazer, G.W., Magnussen, S., Wulder, M.A. and Niemann, K.O., 2011. Simulated impact of sample plot size and co-registration error on the accuracy and uncertainty

of LiDAR-derived estimates of forest stand biomass. Remote Sensing of Environment, 115(2): 636-649. doi:10.1016/j.rse.2010.10.008

Foody, G.M., Boyd, D.S., Cutler, M.E.J., 2003. Predictive relations of tropical forest biomass from Landsat TM data and their transferability between regions. Remote Sensing of Environment 85 (4), 463-474.

Freedman, B., Stinson, G., & Lacoul, P., 2009. Carbon credits and the conservation of natural areas. Environmental Reviews 17, 1-19. doi:10.1139/A08-007

Freitas, S.R., Mello, M.C.S. and Cruz, C.B.M., 2005. Relationships between forest structure and vegetation indices in Atlantic Rainforest. Forest Ecology and Management 218 (1-3), 353-362.

Grohmann, C.H., Steiner, S.S., 2008. SRTM resample with short distance-low nugget kriging. International Journal of Geographical Information Science 22 (8), 895-906.

Guilherme, F. A. G., Morellato, L. P. C., & Assis, M. A., 2004. Horizontal and vertical tree community structure in a lowland atlantic rain forest, southeastern Brazil. Rev. bras. Bot. 27 (4), 725-737.

Guisan, A. and Zimmermann, N.E., 2000. Predictive habitat distribution models in ecology. Ecological Modelling 135 (2-3), 147-186.

Hall, F. G., Bergen, K., Blair, J. B., Dubayah, R., Houghton, R., Hurtt, G., Kellndorfer, J., Lefsky, M., Ranson, J., Saatchi, S., Shugart, H. H., & Wickland, D., 2011. Characterizing 3D vegetation structure from space: Mission requirements. Remote Sensing of Environment 115 (11), 2753-2775.

He, Q.S., Cao, C.X., Chen, E.X., Sun, G.Q., Ling, F.L., Pang, Y., Zhang, H., Ni, W.J., Xu, M., Li, Z.Y., & Li, X.W., 2012. Forest stand biomass estimation using ALOS PALSAR data based on LiDAR-derived prior knowledge in the Qilian Mountain, western China. International Journal of Remote Sensing 33 (3), 710-729.

Helmer, E.H., Lefsky, M.A., Roberts, D.A., 2009. Biomass accumulation rates of Amazonian secondary forest and biomass of old-growth forests from Landsat time series and the Geoscience Laser Altimeter System. Journal of Applied Remote Sensing 3, 033505. DOI: 10.1117/1.3082116

Hudak, A. T., Strand, E. K., Vierling, L. A., Byrne, J. C., Eitel, J. U. H., Martinuzzi, S., & Falkowski, M. J., 2012. Quantifying aboveground forest carbon pools and fluxes from repeat LiDAR surveys. Remote Sensing of Environment 123, 25-40. doi:10.1016/j.rse.2012.02.023

Huete, A.R., Liu, H.Q. and vanLeeuwen, W.J.D., 1997. The use of vegetation indices in forested regions: Issues of linearity and saturation. Igarss '97 - 1997 International Geoscience and Remote Sensing Symposium, Proceedings Vols I-Iv: 1966-1968.

IPCC, 2006. Guidelines for National Greenhouse Gas Inventories. In H. S. Eggleston, L. Buendia, K. Miwa, T. Ngara & K. Tanabe (Eds.). National Greenhouse Gas Inventories Programme, Japan.

IPCC, 2010. Expert Meeting on National Forest GHC Inventories. Eggleston, H.S.; Srivastava, N.; Tanabe, K., Baasansuren, J. (Eds). National Forest GHC Inventories – a Stock Taking. IGES, Japan.

Kane, V., Gillespie, A., Mcgaughey, R., Lutz, J., Ceder, K., Franklin, J., 2008. Interpretation and topographic compensation of conifer canopy self-shadowing. Remote Sensing of Environment 112 (10), 3820–3832.

Kajisa, T., Murakami, T., Mizoue, N., Top, N. and Yoshida, S., 2009. Object-based forest biomass estimation using Landsat ETM+ in Kampong Thom Province, Cambodia. Journal of Forest Research 14 (4), 203-211.

Li, H., Mausel, P., Brondizio, E., Deardorff, D., 2010. A framework for creating and validating a non-linear spectrum-biomass model to estimate the secondary

succession biomass in moist tropical forests. ISPRS Journal of Photogrammetry and Remote Sensing 65 (2), 241-254.

Lira, P.K., Tambosi, L.R., Ewers, R.M., & Metzger, J.P., 2012. Land-use and land-cover change in Atlantic Forest landscapes. Forest Ecology and Management, 278, 80-89. dx.doi.org/10.1016/j.foreco.2012.05.008

Liu, W., Song, C., Schroeder, T. A., & Cohen, W. B., 2008. Predicting forest successional stages using multitemporal Landsat imagery with forest inventory and analysis data. International Journal of Remote Sensing 29 (13), 3855-3872.

Lu, D. S., 2006. The potential and challenge of remote sensing-based biomass estimation. International Journal of Remote Sensing 27 (7), 1297-1328.

Lu, D., Mausel, P., Brondizio, E. and Moran, E., 2002. Assessment of atmospheric correction methods for Landsat TM data applicable to Amazon basin LBA research. International Journal of Remote Sensing 23 (13), 2651-2671.

Lu, D.S., Mausel, P., Brondizio, E., Moran, E., 2004. Relationships between forest stand parameters and Landsat TM spectral responses in the Brazilian Amazon Basin. Forest Ecology and Management 198 (1-3), 149-167.

Main-Knorn, M., Moisen, G.G., Healey, S.P., Keeton, W.S., Freeman, E.A., & Hostert, P., 2011. Evaluating the Remote Sensing and Inventory-Based Estimation of Biomass in the Western Carpathians. Remote Sensing 3, 1427-1446.

doi:10.3390/rs3071427

Mantelli, L.R., Barbosa, J.M. and Bitencourt, M.D., 2011. Assessing ecological risk through automated drainage extraction and watershed delineation. Ecological Informatics 6 (5), 325-331.

Marques, M. C. M., Burslem, D. F. R. P., Britez, R. M., & Silva, S. M., 2009. Dynamics and diversity of flooded and unflooded forests in a Brazilian Atlantic rain forest: a 16-year study. Plant Ecology & Diversity 2 (1), 57-64.

Martin, A.R., Thomas, S.C., 2011. A Reassessment of Carbon Content in Tropical Trees. Plos One 6 (8), e23533. doi:10.1371/journal.pone.0023533

Mathys, L., Guisan, A., Kellenberger, T.W. and Zimmermann, N.E., 2009. Evaluating effects of spectral training data distribution on continuous field mapping performance. Isprs Journal of Photogrammetry and Remote Sensing 64 (6), 665-673.

McCullagh P., Nelder J.A., 1989. Generalized linear models, 2nd ed. Chapman & Hall, London

Munroe, D. K., Nagendra, H., & Southworth, J., 2007. Monitoring landscape fragmentation in an inaccessible mountain area: Celaque National Park, Western Honduras. Landscape and Urban Planning 83 (2-3), 154-167.

Myers, N., Mittermeier, R.A., Mittermeier, C.G., da Fonseca, G.A.B. and Kent, J., 2000. Biodiversity hotspots for conservation priorities. Nature, 403 (6772): 853-858.

Naughton-Treves, L., 2004. Deforestation and Carbon Emissions at Tropical Frontiers: A Case Study from the Peruvian Amazon. World Development 32 (1), 173-190.

Neeff, T., Lucas, R.M., Santos, J.R.d., Brondizio, E.S., Freitas, C.C., 2006. Area and Age of Secondary Forests in Brazilian Amazonia 1978–2002: An Empirical Estimate. Ecosystems 9 (4), 609-623.

O'Brien, R. M., 2007. A caution regarding rules of thumb for variance inflation factors. Quality & Quantity 41 (5), 673-690.

Peroni, N., & Hanazaki, N., 2002. Current and lost diversity of cultivated varieties, especially cassava, under swidden cultivation system in the Brazilian Atlantic Forest. Agriculture, Ecosystems and Environment 92 (2-3), 171-183.

Pfaff, A. and Walker, R., 2010. Regional interdependence and forest "transitions": Substitute deforestation limits the relevance of local reversals. Land Use Policy, 27(2): 119-129.

Pontius, R.G., 2000. Quantification error versus location error in comparison of categorical maps. Photogrammetric Engineering and Remote Sensing 66 (8), 1011-1016.

Ribeiro, M. C., Metzger, J. P., Martensen, A. C., Ponzoni, F. J., & Hirota, M. M., 2009. The Brazilian Atlantic Forest: How much is left, and how is the remaining forest distributed? Implications for conservation. Biological Conservation 142 (6), 1141-1153.

Saatchi, S.S., Houghton, R.A., Dos Santos Alvalá, R.C., Soares, J.V., & Yu, Y., 2007. Distribution of aboveground live biomass in the Amazon basin. Global Change Biology 13 (4), 816-837.

Saatchi, S., Marlier, M., Chazdon, R.L., Clark, D.B., Russell, A.E., 2011. Impact of spatial variability of tropical forest structure on radar estimation of aboveground biomass. Remote Sensing of Environment 115 (11), 2836–2849.

Sarker, L.R. and Nichol, J.E., 2011. Improved forest biomass estimates using ALOS AVNIR-2 texture indices. Remote Sensing of Environment 115 (4), 968-977.

Schwarz, M. and Zimmermann, N.E., 2005. A new GLM-based method for mapping tree cover continuous fields using regional MODIS reflectance data. Remote Sensing of Environment 95 (4), 428-443.

Silva, W.G.d. *et al.*, 2008. Relief influence on tree species richness in secondary forest fragments of Atlantic Forest, SE, Brazil. Acta bot. bras. 22 (2), 589-598.

Sirén, A.H., Brondizio, E.S., 2009. Detecting subtle land use change in tropical forests. Applied Geography 29 (2), 201-211.

Slater, P. N., 1980. Remote sensing: optics and optical systems. Reading, MA, Addison-Wesley, 575p.

Soenen, S.A., Peddle, D.R. and Coburn, C.A., 2005. SCS+C: A modified sun-canopy-sensor topographic correction in forested terrain. IEEE Transactions on Geoscience and Remote Sensing 43(9), 2148-2159.

Soenen, S.A., Peddle, D.R., Hall, R.J., Coburn, C.A., & Hall, F.G., 2010. Estimating aboveground forest biomass from canopy reflectance model inversion in mountainous terrain. Remote Sensing of Environment 114 (7), 1325-1337.

SOS Mata Atlântica, Instituto Nacional de Pesquisas Espaciais (Inpe), 2012. Atlas dos remanescentes florestais da Mata Atlântica, período de 2010 a 2011. <http://www.sosmatatlantica.org.br> (Accessed 30 September, 2012)

Southworth, J., & Tucker, C., 2001. The influence of accessibility, local institutions, and socioeconomic factors on forest cover change in the mountains of western Honduras. Mountain Research and Development 21 (3), 276-283.

Steininger, M.K., 2000. Satellite estimation of tropical secondary forest above-ground biomass: Data from Brazil and Bolivia. International Journal of Remote Sensing 21 (6-7), 1139–1157.

Sun, G., Ranson, K.J., & Kharuk, V.I., 2002. Radiometric slope correction for forest biomass estimation from SAR data in the Western Sayani Mountains, Siberia. Remote Sensing of Environment 79 (2-3), 279-287.

Tabarelli, M., Mantovani, W., 1999. A riqueza de espécies arbóreas na floresta atlântica de encosta no estado de São Paulo (Brasil). Revista Brasileira de Botânica, 22 (2), 217-223.

Tangki, H., & Chappell, N.A., 2008. Biomass variation across selectively logged forest within a 225-km2 region of Borneo and its prediction by Landsat TM. Forest Ecology and Management 256 (11), 1960-1970.

Teixeira, A. M. G., Soares, B. S., Freitas, S. R., & Metzger, J. P., 2009. Modeling landscape dynamics in an Atlantic Rainforest region: Implications for conservation. Forest Ecology and Management 257 (4), 1219-1230.

Valeriano, M. d. M., 2008. Topodata: guia para utilização de dados geomorfológicos locais. In: Instituto Nacional de Pesquisas Espaciais (INPE-15318-RPQ/818), São José dos Campos, SP, Brazil. < http://mtc-m18.sid.inpe.br/col/sid.inpe.br/mtc-m18@80/2008/07.11.19.24/doc/publicacao.pdf> (Accessed 20 September 2012)

Valeriano, M.D., Rossetti, D.D., 2012. Topodata: Brazilian full coverage refinement of SRTM data. Applied Geography 32 (2), 300-309

Valeriano, M.d.M., 2011. Cálculo do fator topográfico de iluminação solar para modelagem ecofisiológica a partir do processamento de Modelos Digitais de Elevação (MDE). In Instituto Nacional de Pesquisas Espaciais (Ed.), XV Simpósio Brasileiro de Sensoriamento Remoto (pp. 5933-5940). Curitiba, PR, Brasil: Instituto Nacional de Pesquisas Espaciais (INPE).

Valeriano, M.d.M., Albuquerque, P.C.G.d., 2010. TOPODATA: processameto dos dados SRTM. In. INPE (Instituto Nacional de Pesquisas Espaciais), São José dos Campos, SP, Brazil, 79 p. < http://mtc-m19.sid.inpe.br/col/sid.inpe.br/mtc-m19@80/2010/05.10.18.42/doc/publicacao.pdf> (Accessed 20 September 2012).

Valeriano, M.M., Kuplich, T.M., Storino, M., Amaral, B.D., Mendes Jr, J.N., Lima, D.J., 2006. Modeling small watersheds in Brazilian Amazonia with shuttle radar topographic mission-90m data. Computers & Geosciences 32 (8), 1169-1181.

Vieira, I. C. G., de Almeida, A.S., Davidson, E.A., Stone, T.A., Reis de Carvalho, C.J., Guerrero, J.B., 2003. Classifying successional forests using Landsat spectral properties and ecological characteristics in eastern Amazônia. Remote Sensing of Environment 87 (4), 470-481.

Vieira, S.A.A., L. F.; Aidar, M.; Araújo, L. S.; Baker, T.; Batista, J. L. F.; Campos, M. C.; Camargo, P. B.; Chave, J.; Delitti, W. B. C.; Higuchi, N.; Honorio, E.; Joly, C. A.; Keller, M.; Martinelli, L. A.; Arcoverde de Mattos, E.; Metzker, T.; Phillips, O.; Santos, F. A. M.; Shimabukuro, M. T.; Silveira, M.; Trumbore, S. E., 2008. Estimation of biomass and carbon stocks: the case of the Atlantic Forest. Biota Neotropica 8 (2), 21-29.

Walker, R., 2012. The scale of forest transition: Amazonia and the Atlantic forests of Brazil. Applied Geography 32 (1), 12-20.

Wang, C., Qi, J., 2008. Biophysical estimation in tropical forests using JERS-1 SAR and VNIR imagery. II. Aboveground woody biomass. International Journal of Remote Sensing 29 (23), 6827-6849

Wijaya, A., Liesenberg, V. and Gloaguen, R., 2010. Retrieval of forest attributes in complex successional forests of Central Indonesia: Modeling and estimation of bitemporal data. Forest Ecology and Management 259 (12), 2315-2326.

Wu, J., Bauer, M.E., Wang, D., Manson, S.M., 2008. A comparison of illumination geometry-based methods for topographic correction of QuickBird images of an undulant area. ISPRS Journal of Photogrammetry and Remote Sensing 63 (2), 223–236.

Zolkos, S.G., Goetz, S.J. and Dubayah, R., 2013. A meta-analysis of terrestrial aboveground biomass estimation using lidar remote sensing. Remote Sensing of Environment 128: 289-298. http://dx.doi.org/10.1016/j.rse.2012.10.017.

CAPÍTULO 4

Combining annual sunlight pattern and remote sensed data to evaluate forest canopy structure

CAPÍTULO 4

Combining annual sunlight pattern and remote sensed data to evaluate forest canopy structure

Jomar Magalhães Barbosa[a], Francisco d'Albertas Gomes de Carvalho[a], Marisa Dantas Bitencourt[a]

[a] Department of Ecology, Institute of Biosciences, University of São Paulo, Brazil.

Abstract:

The use of remote sensing to estimate forest structure has been widely tested, but few studies have modeled canopy closure in tropical forests on steeply sloping terrain. We tested the effect of the annual direct sunlight on forest canopy closure. In addition, we analyzed the potential use of remote sensing data to generate a predictive model for canopy closure in steep-slope areas of the Atlantic Rainforest. Field canopy closure data were collected from 52 sample points. We verified the relationship among the annual direct sunlight, the slope aspect and the canopy closure and subsequently modeled the canopy closure using Landsat TM, Alos Avnir-2 and annual direct sunlight data as explanatory variables. We found a pronounced effect from both the slope aspect and seasonality on the incident pattern of direct solar radiation. The field canopy closure of the sampled points oriented to the north, east and west displayed greater canopy closure than points facing south. The use of annual direct sunlight in conjunction with the TM and Alos data produced the best predictions of the canopy closure. The performances of the TM and ALOS images to estimate canopy closure were similar despite their differences in spatial resolution. The soil/vegetation index suggested in this study performed better than other vegetation indices. The use of a digital elevation model to estimate the annual direct sunlight radiation was found to be a useful source of data in analyzing forest responses to large-scale topographic patterns.

Keywords: remote sensing, canopy closure, sunlight, tropical forest and topography

1 - Introduction

The topographic features and geographic position of a region determine the patterns of incident solar radiation and the consequent changes in environmental conditions (Fu and Rich *et al.*, 2002). During the year, uneven illumination over forest patches can lead to differences in the canopy structure (Dahlin *et al.*, 2012) because the available photosynthetically active radiation (PAR) differs in shaded areas compared with that of sunny areas (Olseth and Skartveit, 1997; Bennie *et al.*, 2008). The arrangement of the tree crown architecture and the leaf area affect the light diffusion and availability throughout the canopy. Thus, the understory illumination depends on the interaction between the canopy closure (canopy gaps) and the amount of sunlight received during the year (Marthews *et al.*, 2008). In all cases, the light availability over different spatial and temporal ranges can lead to a great diversity of microhabitats and helps determine the related ecological and physiological processes (Denslow *et al.*, 1990; Turton and Freiburger, 1997; Suganuma *et al.*, 2008).

Estimations of direct sunlight over forest areas can be obtained from remote sensing data, which may be a useful source of information for eco-physiology studies (Valeriano, 2011). The modeling approaches for sunlight estimation at a landscape scale are primarily based on digital elevation models and sun angles, although they vary in complexity depending on the level of detail required (Flint and Childs, 1987; Allen *et al.*, 2006; Valeriano, 2011). Under the forest canopy, accurate and direct measurements of the understory light regime are expensive and time-consuming. However, one indirect method for obtaining light conditions under the forest canopy is the measurement of the canopy closure, which is the proportion of the sky hemisphere obscured by vegetation as viewed from a single point (Jennings *et al.*, 1999). The canopy closure can be estimated using different methodologies (Lemmon, 1956; Evans

and Coombe, 1959; James 1971; Laymon 1988; O'Brien and Van Hooser 1983), all of which are fairly similar (Laymon, 1988); however, the method chosen depends on the objectives of each study and on the accuracy required (Engelbrecht and Herz, 2001).

Many approaches have been tested for modeling the forest structure using remote sensing data (Freitas *et al.* 2005; Lu, 2006; Lei *et al.*, 2012; Coulston *et al.* 2012), but few studies have used satellite data to generate information on the canopy closure in tropical forests. In this context, the present work aims to test the effect of the annual direct sunlight availability on the forest canopy closure. In addition, the study also analyzes the potential use of remote sensing data to generate a predictive model of canopy closure in steep-slope areas of the Atlantic Rainforest.

2 - Methods

2.1 - Study Area

A field data survey was carried out in the mountainous area of the Ribeira Valley (latitude 24°33’ S and longitude 48°39’ W) located in the south of São Paulo State, Brazil (Figure 1). The area consists of a series of steep ridges ranging from 200 m to 600 m in elevation. The climate is humid sub-tropical, with hot summers and the absence of drought. The mean annual temperature is over 21°C, and rainfall is abundant, up to 1500 mm annually. The vegetation type is defined as Atlantic Rainforest, which is characterized by a high species diversity and complex structural forest canopy layers (Guilherme *et al.*, 2004; Marques *et al.*, 2009).

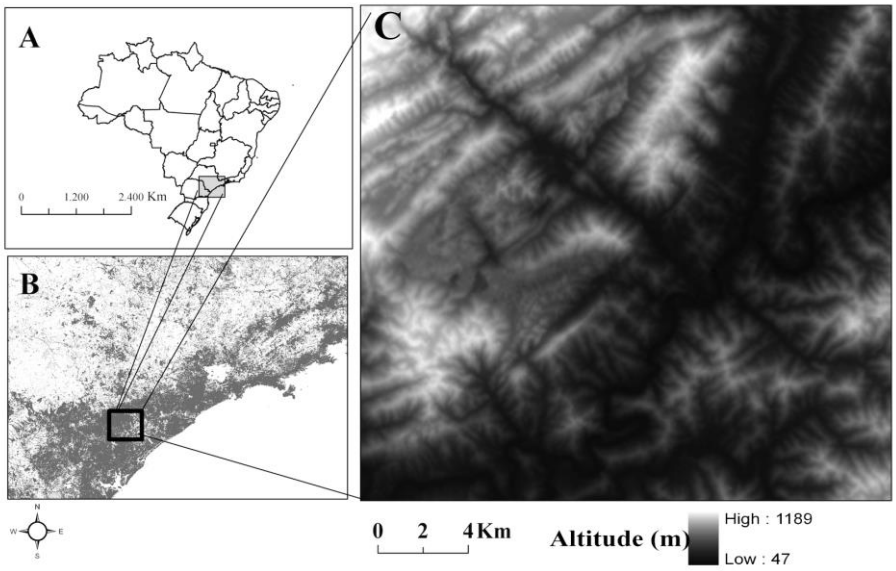

Figure 1. Studied region: (A) study region; (B) the gray color represents the forest cover, and the black square represents the study area; (C) digital elevation model (meters).

The Ribeira Valley encompasses the largest continuous forest patches in the Brazilian Atlantic Rainforest, which are part of the Atlantic Forest Biosphere Reserve (Ribeiro *et al.* 2009). This forest area remains in existence primarily due to unfavorable conditions for intensive agriculture production, such as rugged relief and poor soil (Aidar, 2000). The region has been used for subsistence production by small farmers using slash-and-burn agriculture systems (Adams, 2000; Peroni and Hanazaki, 2002). This management practice has resulted in a heterogeneous forest mosaic comprising different forest regrowth stages.

2.2 - Vegetation inventory data

Vegetation data from 52 sample points were collected during November 2010 over an area of 15,000 ha. The sampled points were distributed among nine classes of a cross-tabulation among three classes of direct solar radiation patterns (illumination factor – IF – see topic 2.3) and three other classes of enhanced vegetation indices (EVI

– topic 2.4). Both sets of data were previously obtained from satellite images and used to guide the field survey. The separation among the IF and EVI classes was constructed by considering the minimal variation within the groups and maximizing the variance between classes. Moreover, the points were proportionally spread over two forest succession stands, namely, an initial secondary forest class (tree height less than 10 m) and an advanced secondary forest/primary forest class (tree height greater than 10 m). The sample points were systematically distributed to account for the heterogeneity of the field vegetation and topographic features.

The forest canopy closure was estimated using a spherical densiometer, a rapid and inexpensive method (Lemmon, 1956) that yields reasonably precise estimation of incident sunlight and is useful for ecological studies (Englund *et al.*, 2000; Tinya *et al.*, 2009). This instrument is composed of a concave mirror with a view angle of 60°. The portion of the sky covered by the canopy was subsequently computed by placing the spherical densitometer in a horizontal position at breast height in each of the 52 sampled points. The canopy closure data obtained from the spherical densiometer were photographed digitally to eliminate the observer subjectivity in scoring canopy closure by visual analysis. The pictures were transformed into binary images (Figure 2) using Sidelook software (Nobis, 2005). The algorithm of the software detects the border between pixels representing the sky and the vegetation as defined by the maximum contrast between them (Nobis and Hunziker, 2005). Finally, the number of black and white pixels was counted using Idrisi Andes® software, producing a canopy closure expressed as percentage value from 0 to 1.

Figure 2. Spherical densiometer image used to estimate the field canopy closure. Black color = forest canopy; white color = open sky.

2.3 - Annual Illumination Factor

The illumination factor at a specific time represents the angle between the direct solar beam and a line normal to the ground (perpendicular to the surface) (Figure 3). The annual illumination factor (AIF) is the mean value of the daily and monthly IF and represents the average illumination conditions as a function of the direct sunlight radiation during the year (Valeriano, 2011). The digital elevation model (DEM) was the primary source of data used to calculate the IF, and the TOPODATA database (http://www.dsr.inpe.br/topodata) was used to obtain the DEM data. The TOPODATA is derived from the Shuttle Radar Topography Mission (SRTM-3) available from the United States Geological Survey (http://dds.cr.usgs.gov/ srtm/version2_1/SRTM3/) refined to a spatial resolution of 30 m (Valeriano and Rossetti 2008).

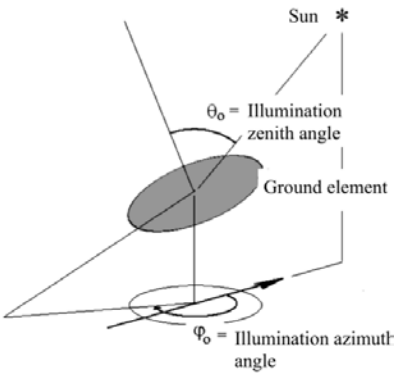

Figure 3. The IF (cos θ_o) of an inclined surface (Adapted from Valeriano, 2011).

The AIF calculation is based on the solar angles (sun azimuth and zenith) controlled by the daily and annual cycles. These daily and annual solar dynamics were estimated using the hour angle (h) and the declination angle (δ), respectively. Next, the sun zenith (θs) and azimuth (φs) at each latitude position were calculated with the following equations:

$$cos\theta_s = sen\, Y\, .\, sen\, \delta + \cos Y\, .\ cos\delta\, .\cos h \quad \text{(eq. 1)}$$

$$sen\, \varphi_s = \frac{\cos\delta\, sen\, h}{sen\, \theta_s} \quad \text{(eq. 2)}$$

where Y is the local latitude. The hour (h) and declination (δ) angles were calculated as a function of local time, the position at the summer solstice in the Southern Hemisphere (-23.45°) and the number of days after January 1st (D):

$$h = 15° \,.\, [local\ time - 12] \quad \text{(eq. 3)}$$

$$\delta = -23.45° \,.\, cos\ ((360°/365)\,.\,(D + 10)) \quad \text{(eq. 4)}$$

The calculations for the φ_s and θ_s values were completed for four different times during the day and for four dates in each of the 12 months, resulting in 384 values for both angles (φ_s and θ_s). A total of 192 instant illumination factors (IF) were calculated using all solar angles (eq. 5) (Slater, 1980):

$$IF = \cos\theta_{x,y} \cos\theta_s + \sin\theta_{x,y} \sin\theta_s \cos(\varphi_s - \varphi_{x,y}) \quad \text{(eq. 5)}$$

where θx,y = slope (°), θs = solar zenith (°), φs= solar azimuth (°) and φx,y = aspect (°). The daily IF is the average of four instant IF values from four times each day. The resulting AIF values for each geographic position represent the mean direct sunlight radiation during the year. The higher AIF values indicate a smaller angle between the solar beam and the line normal to the ground.

2.4 - Satellite data pre-processing

The Landsat TM (November 2010) and Alos Avnir-2 (March 2010) products provided the spectral data used in modeling the canopy closure. The satellite data were converted to surface reflectance values and adjusted for atmospheric effects (Chaves 1996). The Alos images were not topographically corrected due to their elevated pixel size difference compared with those of the DEM images. Topographic correction on the TM data was carried out using the C-correction algorithm (eqs. 6 and 7) and was aimed at minimizing the surface reflectance differences due to the sunlight attenuation generated by steep slopes (Riaño, 2003):

$$\cos i = \cos\theta_{x,y}\cos\theta_s + \sin\theta_{x,y}\sin\theta_s\cos(\varphi_s - \varphi_{x,y}) \quad \text{(eq. 6)}$$

$$L_H = L_T \frac{\cos\theta_s + c}{\mathrm{IFcos}\, i + c} \quad \text{(eq. 7)}$$

where IFcos i = modeling illumination, $\varphi_{x,y}$ = aspect (°), φ_s= solar azimuth (°), $\theta_{x,y}$ = slope (°), θ_s = solar zenith (°), L_H = reflectance of a horizontal surface and L_T = reflectance of an inclined surface. Additionally, $c = a_k/b_k$ is obtained from a linear regression between the reflectance data of each TM band (L_T) and cos i ($L_T = a_k + b_k \cos i$).

The TM and Alos images were also processed to produce the vegetation index (VI) and the leaf area index (LAI). The VI is dimensionless and provides information on the amount and condition of the active photosynthetic portion of the canopy (Huete *et al.*, 1999). These indices do not require assumptions or additional information other than the measurements themselves, resulting in simple data analysis (Huete *et al.*, 1999). The subsequent indices were used to model the canopy closure, the LAI (Duchemin *et al.*, 2006), the normalized difference vegetation indices (Rouse *et al.*, 1974) and the enhanced vegetation indices (Huete *et al.*, 1994; Huete *et al.*, 1997), which were estimated by the following equations:

$$NDVI = \frac{\rho NIR - \rho red}{\rho NIR + \rho red} \quad \text{(eq. 8)}$$

$$LAI = \frac{1 - \log(NDVI)}{-0.54} \quad \text{(eq. 9)}$$

$$EVI = G \frac{\rho NIR - \rho red}{\rho NIR + C_1 \times \rho red - C_2 \times \rho blue + L} \quad \text{(eq. 10)}$$

where NDVI is the normalized difference vegetation index, LAI is the leaf area index, EVI is the enhanced vegetation index, ρ is the atmospherically corrected surface reflectance, L (value = 1) is the canopy background adjustment, C_1 (value = 6) and C_2 (value = 7.5) are the coefficients of the aerosol resistance term (which uses the blue band to correct for aerosol influences in the red band) and G (value = 2.5) is a gain factor.

2.5 - Modeling approaches

The relationships among the AIF, the slope aspect and the canopy closure were verified using Pearson's correlation test. Next, we modeled the canopy closure with a linear regression analysis. The modeling was elaborated using the field forest data as the response variable. The explanatory variables included the LAI, VI, AIF and different combinations of the spectral Landsat TM (TM1, TM2, TM3, TM4, TM5 and TM7) and Alos Avnir-2 (Alos1, Alos2, Alos3 and Alos4) data. All possible models were tested for normality using the Shapiro-Wilk normality test. The model fitness was evaluated using the R-squared (R^2) and root mean square error (RMSE) values. The RMSE compares the ground truth with the modeled data. In this validation procedure, we randomly selected 70% of the total data set (52 field points) with 100 repetitions. In each selection, we obtained the RMSE for comparison of the remaining 30% of the field canopy closure values with the values estimated by the models. Next, we evaluated the reliability of each model using the mean of the 100 RMSE values. All of the statistical

analyses were implemented using the R environment, version 2.0.0 (R Development Core Team, 2011).

3 - Results

3.1 - Annual dynamics of direct sunlight illumination

The daily direct sunlight availability declined between 40% and 90% from the summer to the winter season for the surveyed points oriented to the south (aspect between 120° and 250°). For points facing north, east and west, the daily illumination factor showed minimal reductions over the year, but in a few locations, we found a maximum decrease of 30% in the winter season (Figure 4). The influence of the seasonality, aspect and slope on the daily illumination factor determined the results of the annual availability of the direct sunlight radiation (AIF). The AIF of the studied area ranged from 0.28 to 0.66, with a mean value of 0.51 (SD = 0.09). We found an evident reduction of the annual direct solar radiation in field locations facing to the south (Figure 5). In addition, at intermediary ground slopes, a greater AIF heterogeneity was observed than at low or elevated slopes (Figure 6).

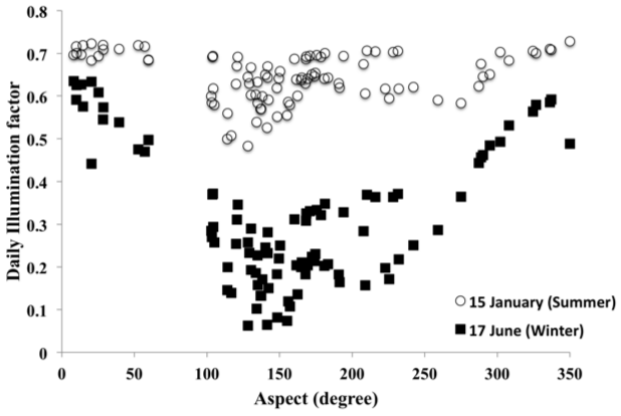

Figure 4. Relationship between the daily illumination factor of all sampled points and the gound aspect in the summer and winter seasons.

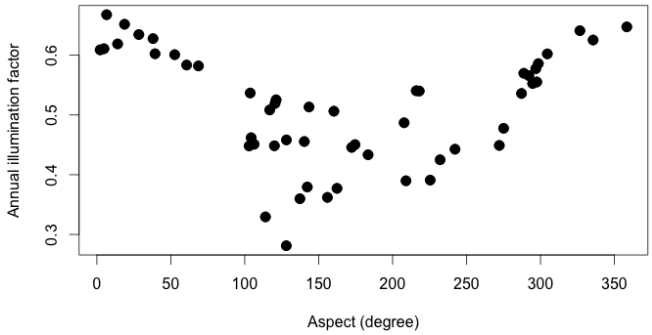

Figure 5. Scatterplot of the ground aspect and the annual illumination factor.

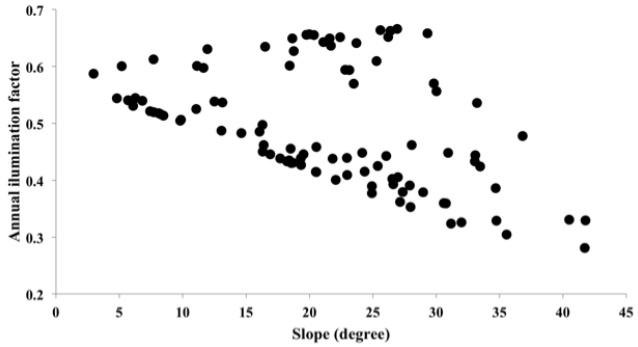

Figure 6. Scatterplot of the ground slope and the annual illumination factor.

3.2 - Field canopy closure

The field canopy closure ranged from 0.58 to 0.97, with a mean value of 0.81 (SD = 0.08). No significant differences ($\rho>0.05$) were found in the canopy closure values between the two analyzed forest succession stands (initial secondary forest and advanced secondary forest). The field canopy closure of the sampled points facing north, east and west showed a tendency toward higher canopy closure than points facing south (Figure 7). This tendency was confirmed with the significant difference of the canopy closure ($\rho = 0.05$) between two separate groups: the north/east/west group and the south group (Figure 8). We also noted a tenuous positive increase between the AIF and canopy closure ($\rho > 0.05$) (Figure 9).

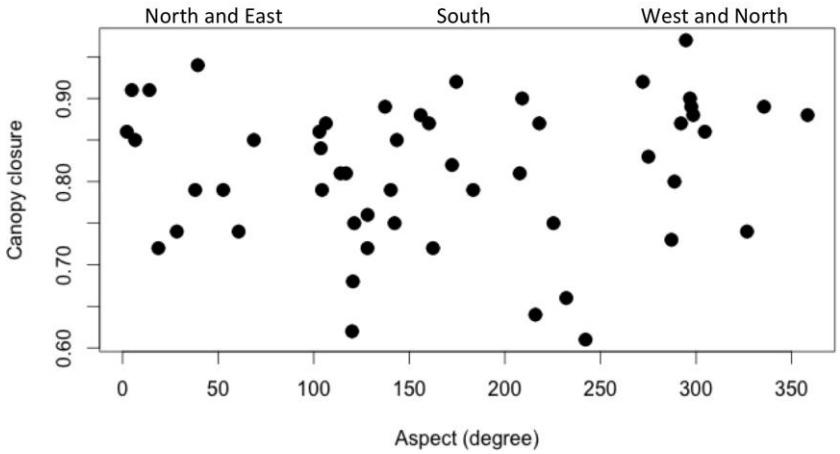

Figure 7. Scatterplot of the canopy closure and aspect (°).

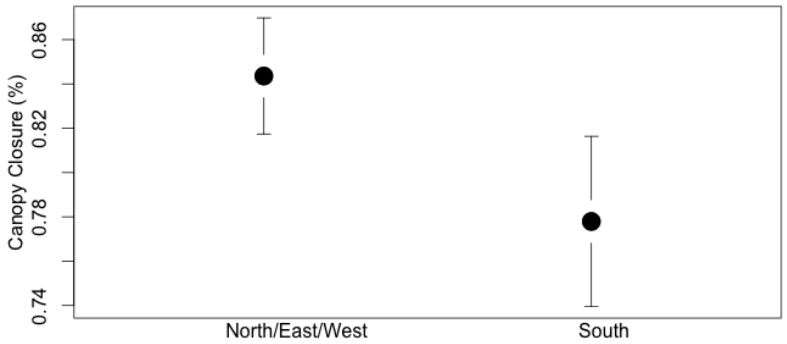

Figure 8. Mean canopy closure of the sampled points located in the north/east/west-facing directions and in the south-facing direction.

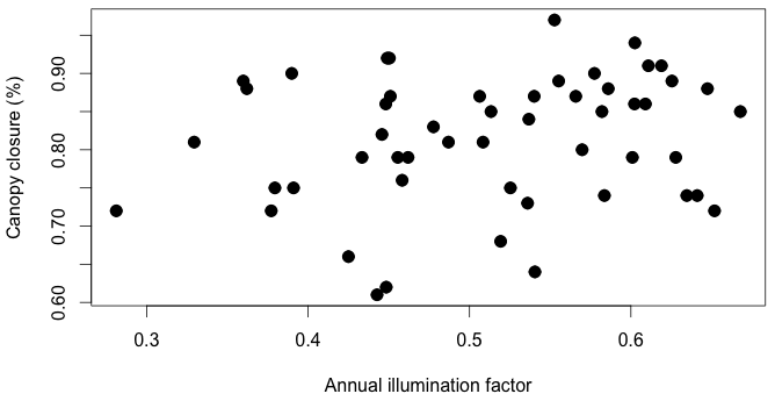

Figure 9. Scatterplot of the canopy closure and annual illumination factor.

3.3 - Modeled canopy closure and prediction accuracy

The use of AIF in conjunction with the TM or Alos data exhibited the best predictions for the canopy closure (Figure 10). In contrast, the use of topographically corrected TM images reduced the performance of the models in estimating the canopy closure. The performances of the TM and ALOS images were similar despite their spatial resolution differences. Two spectral bands, TM 7 (2.08-2.35 μm) and Alos1 (0.42-0.5 μm), exhibited the highest determination coefficient (R^2 = 0.30 and R^2 = 0.28, respectively) for predicting the canopy closure (Table 1). In both cases, the images were modeled in combination with the AIF.

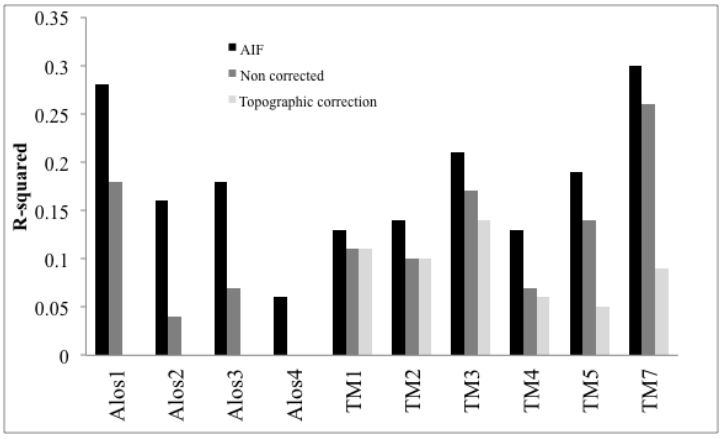

Figure 10. R-squared values for the estimated canopy closure using TM and Alos images. Black bars = modeling with the annual illumination factor; dark gray bars = modeling without the illumination factor; light gray bars = modeling with topographically corrected images and without the illumination factor.

Table 1: Performance of the three best models used to estimate canopy closure.

Equation	**Model**	**R^2**
Eq. 11	Canopy closure = 0.93 + 0.19(AIF) – 3.58 (TM7)	0.30
Eq. 12	Canopy closure = 0.76 + 0.29 (AIF) – 7.29 (Alos1)	0.28
Eq. 13	Canopy closure = 1.13 + 0.14(AIF) – 0.15((TM5+TM7)/(TM5-TM7))	0.23

All indices used to estimate the canopy closure resulted in lower determination coefficients when compared with the satellite image bands alone (Figure 11). However, the soil/vegetation index (Table 1 - eq. 13), elaborated in the present study, exhibited a performance similar to that of the band-alone models. The soil/vegetation index was proposed to take into account the interaction between the satellite spectral responses of the soil (between 2.08-2.35 μm) and the vegetation water content (between 1.55-1.75 μm). The EVI obtained using the TM and ALOS images showed lower R^2 values than those of the other indices. The models "soil/vegetation indices/AIF" and "TM7/AIF" resulted in a canopy closure RMSE of 0.071 and 0.070, respectively. These RMSE values represent an error of approximately 22%, considering the range of 0.58 to 0.97 for the field canopy closure.

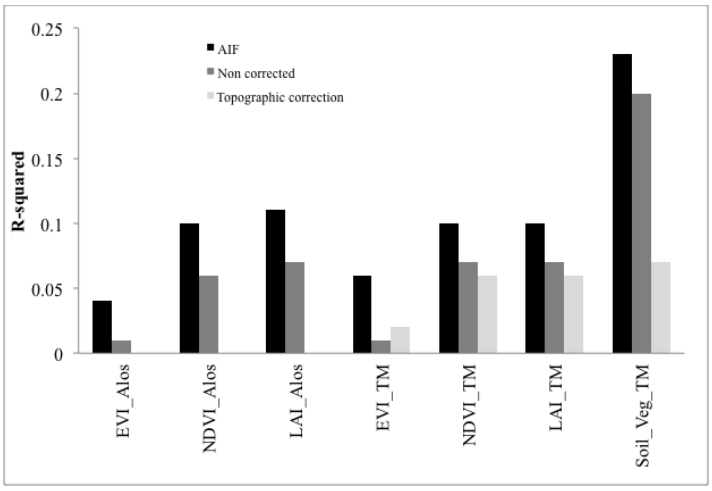

Figure 11. R-squared values for the estimated canopy closure using the enhanced vegetation Index (EVI), normalized difference vegetation index (NDVI), leaf area index (LAI) and normalized soil/vegetation index (Soil_Veg). Black bars = modeling using the annual illumination factor; dark gray bars = modeling without the annual illumination factor; and light gray bars = modeling with topographically corrected images. Alos = Alos images; and TM = Landsat TM images

4 - Discussion

4.1 - Influence of the geomorphology pattern on canopy closure

The results indicate the presence of mountainsides that are shaded for longer periods than others over the year. These illumination differences are mainly determined by the latitude, slope and aspect (Flint and Childs, 1987; Olseth and Skartveit, 1997). In the studied Atlantic Rainforest area, we observed lower annual direct sunlight radiation in the southern areas than in areas facing to the north, east or west. These AIF differences due to the slope aspect can be primarily attributed to the prominent reduction in the amount of direct sunlight illumination in the winter season in areas facing south. Seasonal sunlight changes on the south-facing mountainsides mean that the vegetation must depend on diffuse solar radiation in the winter season (Allen *et al.*, 2006).

We noted higher field canopy closure values on mountainsides facing north, east and west than those facing south. The well-defined differences in canopy closure among the slope aspects can be partially explained by differences in the sunlight availability. Indeed, a positive increase was observed between the field canopy closure and the AIF; however, this relationship was tenuous. Nevertheless, these results suggest an increase in foliage biomass due to the increase in the annual direct sunlight availability.

In tropical forests, the tree growth rate is positively related to the amount of solar radiation (Dong *et al.*, 2012). The more frequent direct sunlight radiance on the north/east/west aspects enable a greater penetration of sunlight through the upper canopy. This greater amount of sunlight enhances leaf growth (Ackerly and Bazzaz, 1995), elevates the number of canopy layers and increases the canopy closure. In contrast, the reduced AIF on the south-facing slopes may result in a smaller carbon investment and lower foliage density under decreased PAR (Baldocchi *et al.*, 2002),

which can occur because much of the attenuation and interception of the PAR takes place primarily in the upper leaf layers of the canopy (Flint and Caldwell, 1998).

In addition to the importance of light availability to the photosynthetic process, other micro-scale environmental conditions (i.e., soil properties, soil moisture, human management and species composition) may also determine the canopy closure. In addition, the weak estimations of the canopy closure using the modeled sunlight pattern may be related to errors in the slope, aspect and the derived viewshed obtained from the DEM data (Fu and Rich *et al.*, 2002).

Despite the suggested limitations in the use of the spherical densiometer for analysis of the canopy structure (Engelbrecht and Herz, 2001), our results are similar to results taken from digital cameras attached to a fish-eye lens (Lima and Gandolfi, 2009). The coarse spatial scale of the present study enables the meaningful use of the spherical densiometer to evaluate light availability below the forest canopy (Englund *et al.*, 2000).

4.2 – Modeled canopy closure

The canopy closure predictions showed better results when the annual direct solar radiation (i.e., AIF) was modeled together with the satellite data. First, the AIF is able to modulate the topographic influence on the modeling of the canopy structure. Second, this explanatory variable can minimize the reflectance differences in the satellite images with respect to topographic shading. In other studies, the inclusion of the topographic data in the modeling steps increased the accuracy of the forest biomass estimation (Soenen *et al.*, 2010; Main-Knorn *et al.*, 2011). In contrast, the use of topographic correction on the TM images did not result in better canopy closure estimations compared with models that used the AIF. The topographic corrections are attenuations of the topographic distortions in the images and may expose limitations in

the reduction of all topographic effects (Song and Woodcock, 2003; He *et al.*, 2012).

The better performance of the Alos blue band (0.42-0.5 μm) and TM7 mid-infrared band (2.08-2.35 μm) is similar to results obtained by Lei *et al.* (2012). The amounts of soil moisture, hydroxyl ions and iron oxide in the soil have a significant influence on the TM7 reflectance (Baumgardner *et al.*, 1985). In addition, Demattê *et al.* (2010) found a stronger relationship between the soil attributes (i.e., clay and sand content) and the variation in the reflected electromagnetic energy at the 2.2-2.3 μm wavelengths. Canopy gaps and changes in the leaf area and biomass determine the canopy closure pattern because these factors affect the percentage of the exposed substrate (soil, rocks, litter), which can create changes in the patterns of the middle-infrared reflectance.

Vegetation indices derived from satellite images have been widely used to detect changes in the forest canopy structure (Huete *et al.*, 1997; Huete *et al.*, 2002). However, we identified better canopy closure predictions using the soil/vegetation index, which integrates data from the soil (TM7) and water content (TM5) reflectance. In general, the use of indices is more favorable than the spectral bands alone because they are based on the ratio between data from different spectral ranges, which can reduce multiplicative noise (illumination differences, cloud shadows, atmospheric attenuation and topographic variations) (Huete *et al.*, 2002).

Anaya *et al.* (2009) also found no significant relationship between the EVI and tropical forest biomass. Despite the EVI improvements over the NDVI (Huete *et al.*, 1997), the EVI continues to perform less effectively in the evaluation of dense forest areas. The intermediary leaf biomass and the canopy stratification result in rapid absorption of the visible spectral interval and rapid saturation of the vegetation indices (Huete *et al.*, 1997). In the EVI formula, the coefficients and the blue band should

reduce the saturation, thus minimizing the reflectance effect from the soil and the atmosphere and placing additional weight on the near-infrared reflectance (Huete *et al.*, 1997). Nonetheless, the poor model performance of the EVI can be explained in part by the structural complexity of the tropical forests. Studies with less biodiversity and structurally less complex forests have produced more accurate models (Carreiras *et al.*, 2006; Joshi *et al.*, 2006).

We tested two spatial resolution images, the 30-m (Landsat TM) and 10-m (Alos) resolutions, but the lower pixel size did not result in better canopy closure estimations. Alternatively, the use of images with high spectral and radiometric resolutions might ensure more accurate results (Levesque and King, 2003; Chubey *et al.*, 2006; Falkowski *et al.*, 2009) and should be further tested.

5 – Conclusion

In this study, the topographic roughness of the studied Atlantic Rainforest area was shown to be the determinant of the canopy closure pattern, and the topographic influence on the canopy closure may be attributed to changes in the annual direct solar radiation. The Atlantic Rainforest is distributed over a large range of latitudes, between approximately 5° and 30° (Ribeiro *et al.*, 2009). Consequently, the observed effect of the sunlight regime on the vegetation, as modulated by the topography, might differ significantly over this large latitude range.

The use of a digital elevation model to estimate the annual direct sunlight radiation proved to be a useful source of data to analyze the forest responses to large-scale topographic patterns. The results were sufficiently plausible to encourage further applications, even with the possible limitations of the methodologies, such as the absence of information on the frequency of cloudy days and diffuse illumination. Future

research can determine whether the weak relationship between the AIF and canopy closure is due to a lack of information on the modeling of solar radiation (e.g., diffuse solar radiation) or other micro-scale environmental conditions, such as soil properties, human management and species composition.

Although vegetation indices are typically used to evaluate or estimate forest structures, other indices can be proposed depending on the specific field data under analysis. For example, the canopy closure, openness or gaps may be more effectively analyzed by integrating the soil reflectance and leaf reflectance.

Acknowledgment

Authors are grateful to Sergio Tadeu Meirelles for commenting on earlier versions of this manuscript. Our thanks to Coordenação de Aperfeiçoamento de Pessoal de Nível Superior (CAPES) for the scholarship.

6 - References

Ackerly, D.D., Bazzaz, F.A., 1995. Seedling Crown Orientation and Interception of Diffuse-Radiation in Tropical Forest Gaps. Ecology 76, 1134-1146.

Adams, C., 2000. As roças e o manejo da Mata Atlântica pelos caiçaras: uma revisão. Interciência 25, 143-150.

Aidar, M.P.N., 2000. Ecofisiologia das estratégias de utilização de niotrogênio em arvores da floresta neotropical, Instituto de Biologia. Universidade de Campinas, Campinas, p. 151.

Allen, R.G., Trezza, R., Tasumi, M., 2006. Analytical integrated functions for daily solar radiation on slopes. Agricultural and Forest Meteorology 139, 55-73.

Anaya, J.A., Chuvieco, E., Palacios-Orueta, A., 2009. Aboveground biomass assessment in Colombia: A remote sensing approach. Forest Ecology and Management 257, 1237-1246.

Baldocchi, D.D., Wilson, K.B., Gu, L.H., 2002. How the environment, canopy structure and canopy physiological functioning influence carbon, water and energy fluxes of a temperate broad-leaved deciduous forest-an assessment with the biophysical model CANOAK. Tree Physiology 22, 1065-1077.

Baryla, J., Broz, E., Czylok, A., Michalewska, A., Nikel, A., Nobis, M., Piwowarczyk, R., Poloczek, A., 2005. Typha laxmannii Lepech. The new, expansive kenophyte in Poland: Distribution and taxonomy. Acta Societatis Botanicorum Poloniae 74, 25-28.

Baumgardner, M.F., Silva, L.F., Biehl, L.L., Stoner, E.R., 1985. Reflectance Properties of Soils. Advances in Agronomy 38, 1-44.

Bennie, J., Huntley, B., Wiltshire, A., Hill, M.O., Baxter, R., 2008. Slope, aspect and climate: Spatially explicit and implicit models of topographic microclimate in chalk grassland. Ecological Modeling 216, 47-59.

Carreiras, J.M.B., Pereira, J.M.C., Pereira, J.S., 2006. Estimation of tree canopy cover in evergreen oak woodlands using remote sensing. Forest Ecology and Management 223, 45-53.

Chavez Jr., P.S., 1996. Image-Based Atmospheric Corrections – Revisited and Improved. Photogrammetric Engineering & Remote Sensing 62, 1025 – 1036.

Chubey, M.S., Franklin, S.E., Wulder, M.A., 2006. Object-based analysis of Ikonos-2 imagery for extraction of forest inventory parameters. Photogrammetric Engineering and Remote Sensing 72, 383-394.

Coulston, J.W., Moisen, G. G., Wilson, B. T., Finco, M. V., Cohen, W. B., Brewer, C. K., 2012. Modeling Percent Tree Canopy Cover : A Pilot Study. Photogrammetric Engineering & Remote Sensing 78, 715–727.

Dahlin, K.M., Asner, G.P., Field, C.B., 2012. Environmental filtering and land-use history drive patterns in biomass accumulation in a mediterranean-type landscape. Ecological Applications 22, 104-118.

Dematte, J.A.M., Fiorio, P.R., Araujo, S.R., 2010. Variation of Routine Soil Analysis When Compared with Hyperspectral Narrow Band Sensing Method. Remote Sensing 2, 1998-2016.

Denslow, J.S., Schultz, J.C., Vitousek, P.M., Strain, B.R., 1990. Growth-Responses of Tropical Shrubs to Treefall Gap Environments. Ecology 71, 165-179.

Dong, S.X., Davies, S.J., Ashton, P.S., Bunyavejchewin, S., Supardi, M.N.N., Kassim, A.R., Tan, S., Moorcroft, P.R., 2012. Variability in solar radiation and temperature explains observed patterns and trends in tree growth rates across four tropical forests. Proceedings of the Royal Society B-Biological Sciences 279, 3923-3931.

Duchemin, B., Hadria, R., Erraki, S., Boulet, G., Maisongrande, P., Chehbouni, A., Escadafal, R., Ezzahar, J., Hoedjes, J.C.B., Kharrou, M.H., Khabba, S., Mougenot, B., Olioso, A., Rodriguez, J.C., Simonneaux, V., 2006. Monitoring wheat phenology and irrigation in Central Morocco: On the use of relationships between evapotranspiration, crops coefficients, leaf area index and remotely-sensed vegetation indices. Agricultural Water Management 79, 1-27.

Engelbrecht, B.M.J., Herz, H.M., 2001. Evaluation of different methods to estimate understorey light conditions in tropical forests. Journal of Tropical Ecology 17, 207-224.

Englund, S.R., O'Brien, J.J., Clark, D.B., 2000. Evaluation of digital and film hemispherical photography and spherical densiometry for measuring forest light

environments. Canadian Journal of Forest Research-Revue Canadienne De Recherche Forestiere 30, 1999-2005.

Evans, G.C., Coombe, D.E., 1959. Hemispherical and Woodland Canopy Photography and the Light Climate. Journal of Ecology 47, 103-&.

Falkowski, M.J., Wulder, M.A., White, J.C., Gillis, M.D., 2009. Supporting large-area, sample-based forest inventories with very high spatial resolution satellite imagery. Progress in Physical Geography 33, 403-423.

Flint, A.L., Childs, S.W., 1987. Calculation of Solar-Radiation in Mountainous Terrain. Agricultural and Forest Meteorology 40, 233-249.

Flint, A.L., Childs, S.W., 1987. Calculation of Solar-Radiation in Mountainous Terrain. Agricultural and Forest Meteorology 40, 233-249.

Flint, S.D., Caldwell, M.M., 1998. Solar UV-B and visible radiation in tropical forest gaps: measurements partitioning direct and diffuse radiation. Global Change Biology 4, 863-870.

Flint, S.D., Caldwell, M.M., 1998. Solar UV-B and visible radiation in tropical forest gaps: measurements partitioning direct and diffuse radiation. Global Change Biology 4, 863-870.

Freitas, S.R., Mello, M.C.S., Cruz, C.B.M., 2005. Relationships between forest structure and vegetation indices in Atlantic Rainforest. Forest Ecology and Management 218, 353-362.

Freitas, S.R., Mello, M.C.S., Cruz, C.B.M., 2005. Relationships between forest structure and vegetation indices in Atlantic Rainforest. Forest Ecology and Management 218, 353-362.

Fu, P.D., Rich, P.M., 2002. A geometric solar radiation model with applications in agriculture and forestry. Computers and Electronics in Agriculture 37, 25-35.

Fu, P.D., Rich, P.M., 2002. A geometric solar radiation model with applications in agriculture and forestry. Computers and Electronics in Agriculture 37, 25-35.

Guilherme, F.A.G.M., L. Patrícia C. and ASSIS, Marco A., 2004. Horizontal and vertical tree community structure in a lowland Atlantic Rainforest, southeastern Brazil. Revista Brasileira de Botânica 27, 725-737.

He, Q.S., Cao, C.X., Chen, E.X., Sun, G.Q., Ling, F.L., Pang, Y., Zhang, H., Ni, W.J., Xu, M., Li, Z.Y., Li, X.W., 2012. Forest stand biomass estimation using ALOS PALSAR data based on LiDAR-derived prior knowledge in the Qilian Mountain, western China. International Journal of Remote Sensing 33, 710-729.

Huete, A., Didan, K., Miura, T., Rodriguez, E.P., Gao, X., Ferreira, L.G., 2002. Overview of the radiometric and biophysical performance of the MODIS vegetation indices. Remote Sensing of Environment 83, 195-213.

Huete, A., Justice, C., Liu, H., 1994. Development of Vegetation and Soil Indexes for Modis-Eos. Remote Sensing of Environment 49, 224-234.

Huete, A.J.C., Van Leeuwen, W., 1999. Modis Vegetation Index Algorithm Theoretical Basis. University of Arizona, Tucson, p. 122.

Huete, A.R., Liu, H.Q., Batchily, K., vanLeeuwen, W., 1997. A comparison of vegetation indices global set of TM images for EOS-MODIS. Remote Sensing of Environment 59, 440-451.

James, F.C., 1971. Ordination of habitat relationships among breeding birds. The Wilson Bulletin 83, 215-226.

Jennings, S.B., Brown, N.D., Sheil, D., 1999. Assessing forest canopies and understorey illumination: canopy closure, canopy cover and other measures. Forestry 72, 59-73.

Joshi, C., De Leeuw, J., Skidmore, A.K., van Duren, I.C., van Oosten, H., 2006. Remotely sensed estimation of forest canopy density: A comparison of the performance of four methods. International Journal of Applied Earth Observation and Geoinformation 8, 84-95.

Krumbholz, K., Nobis, E., Shah, N.J., Fink, G.R., 2005. Executive control of spatial selective attention in the visual and auditory modalities activates common cortical areas. Journal of Cognitive Neuroscience, 16-16.

Laymon, S.A., 1988. The ecology of the spotted owl in the central Sierra Nevada, California. University of California, Berkeley, p. 285.

Lei, C., Ju, C., Cai, T., Jing, X., Wei, X., Di, X. , 2012. Estimating canopy closure density and above-ground tree biomass using partial least square methods in Chinese boreal forests. Journal of Forestry Research 23, 191–196.

Lemmon, P.E., 1956. A Spherical Densiometer for Estimating Forest Overstory Density. Forest Science 2, 314–320.

Levesque, J., King, D.J., 2003. Spatial analysis of radiometric fractions from high-resolution multispectral imagery for modeling individual tree crown and forest canopy structure and health. Remote Sensing of Environment 84, 589-602.

Lu, D.S., 2006. The potential and challenge of remote sensing-based biomass estimation. International Journal of Remote Sensing 27, 1297-1328.

Main-Knorn, M., Moisen, G.G., Healey, S.P., Keeton, W.S., Freeman, E.A., Hostert, P., 2011. Evaluating the Remote Sensing and Inventory-Based Estimation of Biomass in the Western Carpathians. Remote Sensing 3, 1427-1446.

Marques, M.C.M., Burslem, D.F.R.P., Britez, R.M., Silva, S.M., 2009. Dynamics and diversity of flooded and unflooded forests in a Brazilian Atlantic rain forest: a 16-year study. Plant Ecology & Diversity 2, 57-64.

Marthews, T.R., Burslem, D.F.R.P., Phillips, R.T., Mullins, C.E., 2008. Modeling Direct Radiation and Canopy Gap Regimes in Tropical Forests. Biotropica 40, 676-685.

Nobis, M., 2005. Sidelook 1.1, 1.1 ed, pp. Imaging software for the analysis of vegetation structure with true-colors photographs.

Nobis, M., Hunziker, U., 2005. Automatic thresholding for hemispherical canopy-photographs based on edge detection. Agricultural and Forest Meteorology 128, 243-250.

O'Brien, R.; Van Hooser, D. D., 1983. Understory vegetation inventory: An efficient procedure. Ogden: United States Department of Agriculture, Forest Service, p. 6. (USDA- INT-323).

Olseth, J.A., Skartveit, A., 1997. Spatial distribution of photosynthetically active radiation over complex topography. Agricultural and Forest Meteorology 86, 205-214.

Peroni, N., & Hanazaki, N., 2002. Corrent and lost diversity of cultivated varieties, especially cassava, under swidden cultivation system in the Brazilian Atlantic Forest. Agriculture, Ecosystems and Environment 92, 171-183.

Riano, D., Chuvieco, E., Salas, J., Aguado, I., 2003. Assessment of different topographic corrections in Landsat-TM data for mapping vegetation types (2003). Ieee Transactions on Geoscience and Remote Sensing 41, 1056-1061.

Ribeiro, M.C., Metzger, J.P., Martensen, A.C., Ponzoni, F.J., Hirota, M.M., 2009. The Brazilian Atlantic Forest: How much is left, and how is the remaining forest distributed? Implications for conservation. Biological Conservation 142, 1141-1153.

Rouse, J.W., R.H. Haas, J.A. Schell, D.W. Deering, J.C. Harlan. , 1974. Monitoring the vernal advancement of retrogradation (greenwave effect) of natural vegetation, NASA/GSFC, Type III, Final Report, Greenbelt, MD, p. 371.

Slater, P.N., 1980. Remote sensing: optics and optical systems. Addison-Wesley Educational Publishers Inc.

Soenen, S.A., Peddle, D.R., Hall, R.J., Coburn, C.A., Hall, F.G., 2010. Estimating aboveground forest biomass from canopy reflectance model inversion in mountainous terrain. Remote Sensing of Environment 114, 1325-1337.

Song, C.H., Woodcock, C.E., 2003. Monitoring forest succession with multitemporal Landsat images: Factors of uncertainty. Ieee Transactions on Geoscience and Remote Sensing 41, 2557-2567.

Suganuma, M.S.T., J. M. D.; C., A. L.; Vanzela, A. L. L.; Benato, T., 2008. Comparando Metodologias para Avaliar Cobertura do Dossel e a Luminosidade no sub-bosque de um Reflorestamento e uma Floresta Madura. Revista Árvore 32, 377-385.

Tinya, F., Mihok, B., Marialigeti, S., Mag, Z., Odor, P., 2009. A comparison of three indirect methods for estimating understory light at different spatial scales in temperate mixed forests. Community Ecology 10, 81-90.

Turton, S. M.; Freiburger, H. J., 1997. Edge and aspect effects on the microclimate of a small tropical forest remnant on the Atherton Tableland, northeastern Australia, In: Laurence, W.F.B., R. O, Tropical forest remmants. University of Chicago, Chicago, pp. 45-54.

Valeriano, M.M., 2011. Cálculo do fator topográfico de iluminação solar para modelagem ecofisiológica a partir do processamento de Modelos Digitais de Elevação (MDE), XV Simpósio Brasileiro de Sensoriamento Remoto. Instituto Nacional de Pesquisas Espaciais (INPE), Curitiba, PR, Brasil.

Valeriano, M.M., Rossetti, D.F., 2008. Topographic modeling of Marajó Island with SRTM data. Revista Brasileira de Geomorfologia 9, 53–63.

CAPÍTULO 5

Considerações Finais:

Síntese dos resultados & discussão geral

1 - Considerações Finais

Nesta tese foram reunidas importantes informações sobre o uso do sensoriamento remoto na estimativa de dados biofísicos de Mata Atlântica. Foi avaliado o efeito do relevo na modelagem de biomassa e fechamento de dossel. Além disso, foi discutido papel da topografia na incidência de radiação solar direta sobre áreas florestadas e sua influência sobre a estrutura do dossel de Mata Atlântica. Um ponto crucial para atingir os objetivos propostos na tese foi integrar o conhecimento teórico e metodológico de duas grandes áreas: a Ecologia e o Sensoriamento remoto.

No capítulo 2 foi feita uma detalhada revisão de literatura sobre os principais aspectos ligados à estimativa de biomassa em florestas tropicais. Foram revisados diversos artigos científicos que enfocam métodos de modelagem da biomassa florestal acima do solo. Foi apresentado o estado atual das técnicas utilizadas na estimativa de biomassa florestal com sensores remotos. Além disso, foram levantados os temas ecológicos discutidos nos artigos e enfocou-se o potencial uso das estimativas de biomassa no estudo de sucessão florestal. Este capítulo forneceu toda a base teórica e prática necessária para a elaboração dos capítulos subsequentes.

Os capítulos 3 e 4 avaliaram a acurácia e precisão de diferentes modelos de estimativa de biomassa e fechamento do dossel, respectivamente, em Mata Atlântica. De uma maneira geral, ambos os capítulos procuram responder questões metodológicas necessárias para uma efetiva avaliação das características biofísicas da vegetação por meio de sensores remotos. O capítulo 4 vai além do enfoque metodológico ao avaliar o efeito dos padrões do relevo sobre a radiação solar incidente e a estrutura do dossel.

Neste capítulo final são reapresentados os principais resultados obtidos nos diferentes estudos que compõem a tese. Os resultados estão listados de forma integrada com o objetivo de fornecer informação base para a discussão e conclusão geral.

2 - Síntese dos principais resultados

Sobre aspectos ecológicos:

- A biomassa florestal estimada por meio de sensores remotos tem sido usada como variável ecológica em diferentes tipos de estudos, como por exemplo: de manejo florestal, estado de conservação de áreas naturais, estimativa de estoques de carbono e no estudo da relação entre condições ambientais e estrutura florestal;

- A modelagem de biomassa de Mata Atlântica apresentou grande diferença entre classes inicial e avançada de sucessão florestal, indicando sua possibilidade de uso na caracterização biofísica da vegetação no processo de sucessão;

- No entanto, os erros nas estimativas de biomassa por meio de imagens de satélite podem limitar a detecção do avanço da sucessão florestal em um curto intervalo temporal;

- Foi observado um maior fechamento do dossel em áreas florestadas voltadas para norte/oeste/leste do que áreas voltadas para sul.

Sobre aspectos técnicos e metodológicos:

- As incertezas nas estimativas de biomassa florestal são determinadas por decisões metodológicas (amostragem, processamento dos dados, modelagem), limitações tecnológicas (tipo de sensor escolhido) e complexidade estrutural da vegetação;

- Diversos sensores têm sido usados na estimativa de biomassa. O LiDAR e radares são amplamente citados como ferramentas mais eficientes para o estudo da estrutura da vegetação. No entanto, as imagens ópticas, como por exemplo, as do Landsat, são as mais utilizadas na literatura levantada. Isso porque limitações de disponibilidade e preço dos dados de LiDAR, além do grande efeito do relevo em imagens de radar, dificultam o uso desses produtos;

- As estimativas de biomassa florestal e fechamento do dossel, por meio de sensores remotos e em área com grande complexidade de relevo, foram mais eficazes quando dados topográficos foram incluídos nos modelos. A integração de dados de infravermelho médio, no intervalo espectral entre 1,55 e 1,75 μm, com uma variável geomorfométrica secundária (Fator de iluminação) resultou em melhores estimativas de biomassa em área de Mata Atlântica. E o uso de dados de infravermelho médio (no intervalo entre 2,08 - 2,35 μm) também integrado com o fator de iluminação resultou na melhor estimativa de fechamento do dossel;

- As correções topográficas das imagens de satélite não foram eficazes na modelagem de estrutura florestal na região estudada (área com topografia altamente irregular);

- O erro obtido no processo de modelagem de biomassa acima do solo em Mata Atlântica foi de 35 Mg/ha (Adj. $R^2 = 0.67$).

- O desempenho da estimativa de fechamento de dossel utilizando imagens tanto imagens Landsat TM quanto ALOS foi baixo.

3 - Discussão geral

A tese avaliou o uso de sensores remotos na estimativa de dois importantes componentes estruturais dos ambientes florestais: o dossel e o estoque de biomassa. De uma maneira geral, existe uma crescente demanda mundial (IPCC, 2006; IPCC, 2010; FAO, 2011) e em Mata Atlântica (Ministério do Meio Ambiente, 2011) por técnicas que possibilitem estimar estoques de biomassa e carbono florestais em escala de paisagem. Isto porque, a manutenção e incremento dos estoques de carbono na vegetação, podem auxiliar na regulação dos gases de efeito estufa, servindo como um serviço ecossistêmico (Grace, 2004). Por outro lado, a modelagem espacialmente explícita do

fechamento do dossel permite inferir variações na abertura de clareiras, complexidade estrutural do dossel e também deciduidade (Bianchini *et al.*, 2001).

As metodologias e enfoques utilizados nos diferentes capítulos ainda são escassos ou inéditos nos estudos em Mata Atlântica. Essa escassez pode ser explicada pela maior atenção dada à Amazônia e também devido a dificuldade de processamento de dados em áreas declivosas. Os resultados obtidos na tese permitiram ampliar o conhecimento sobre o uso de dados de sensores remotos em Mata Atlântica, visto que grande parte dos seus remanescentes florestais estão localizados em áreas declivosas.

Modelos numéricos do relevo serviram de base para modelar os padrões de iluminação solar da área de estudo. Com estes dados, foi possível inferir o efeito da diferença de iluminação solar sobre as estimativas de biomassa e fechamento do dossel. Ao estudar estas variáveis, foram mostradas no decorrer dos capítulos as vantagens e desafios em utilizar o sensoriamento remoto no estudo biofísico da vegetação.

A modelagem de estruturas florestais em nível de escala de paisagem foi feita a partir da integração entre dados categóricos (classes sucessionais) e contínuos (biomassa e fechamento do dossel) provenientes de imagens de satélite. Demonstramos que dentro de uma mesma classe de cobertura florestal (ex. sucessão florestal) podemos observar áreas com valores médios de biomassa modelada bastante distintos entre si. A combinação de dados categóricos e contínuos aumenta bastante o poder de avaliação da estrutura e dinâmica da paisagem (Cassidy *et al.*, 2013).

Muitos modelos de estimativa de biomassa são específicos para uma única região (Asner *et al.*, 2003). Para minimizar este problema, devem ser criados novos métodos que permitam uma rápida calibração e validação de modelos em uma ampla região geográfica (Defibaugh y Chávez and Tullis, 2013). A metodologia de ponto

quadrante pode auxiliar neste processo de validação das estimativas de biomassa, desde que sejam consideras suas limitações na estimativa de densidade de árvores.

4 - Estudos futuros

Apesar das limitações impostas pelo relevo no uso dos sensores remotos, foi feita uma estimativa de biomassa florestal com uma boa acurácia. Os modelos propostos podem ser testados em outras regiões que possuem florestas secundárias de Mata Atlântica, observando se há a manutenção da eficiência nas estimativas. Ou mesmo, estudos futuros podem gerar novas equações, utilizando diferentes tipos de satélites, baseadas na premissa de inclusão de dados de relevo no processo de modelagem.

Foi possível observar uma grande influência das etapas de processamento dos dados na eficácia das estimativas. Por isso, o aperfeiçoamento do processamento de imagens e modelagem estatística são campos de pesquisa ainda abertos. Apesar do grande número de estudos de estimativa de biomassa e carbono em florestas tropicais de todo o mundo, ainda carece de mais estudos regiões com maior representatividade de florestas secundárias, como a Mata Atlântica. O aperfeiçoamento das diferentes ferramentas utilizadas para estimar biomassa florestal é de grande interesse para avaliar os serviços ecossistêmicos de uma região. Neste sentido, a análise temporal de estimativas de biomassa por sensores remotos possui grande potencial para entender como determinadas paisagem se comportam como sumidouros ou fontes de carbono.

Encontramos uma evidente relação entre o padrão topográfico (orientação de vertente) e o fechamento do dossel. Os processos biológicos associados ao padrão encontrado poderiam ser futuramente estudados considerando o efeito de condições ambientais em microescala, propriedades do solo e a ação humana.

Os dados sobre as características biofísicas das áreas florestais, estimadas por sensores remotos, possibilitam responder diferentes questões ecológicas na escala de paisagem. Como por exemplo, na avaliação da degradação de fragmentos florestais e do efeito da estrutura da paisagem (fragmentação, conectividade, isolamento, etc.) sobre a estrutura biofísica da vegetação.

5 - Conclusões gerais

- Existem grandes desafios no aumento da acurácia dos modelos que estimam estrutura florestal por meio do sensoriamento remoto. Por isso, existe um grande número de estudos científicos voltados para um enfoque metodológico, o que resulta em um baixo número publicações que respondem perguntas ecológicas utilizando os dados modelados. A escolha da fonte de dados a ser usada nos modelos depende de "tradeoffs" entre vantagens e desvantagens no uso de cada satélite;

- A inclusão de dados geomorfológicos no processo de modelagem da biomassa de áreas declivosas melhora a acurácia dos resultados. A modelagem da biomassa florestal por meio de sensores remotos possibilita avaliar diferenças estruturais entre e dentro dos estágios sucessionais de regeneração florestal;

- Os padrões de fechamento de dossel variaram juntamente com características topográfica existente na área de Mata Atlântica estudada. Esta relação pode ser atribuída a mudanças na radiação anual direta sobre as diferentes faces dos morros. Apesar de os índices de vegetação serem amplamente usados para avaliar estrutura de dossel florestal, ao estudar o fechamento de dossel foi encontrado melhores resultados utilizando um índice que usa informação conjunta da refletância foliar e do solo.

6 - Bibliografia

Asner, G.P.; Hicke, J.A.; Lobell, D.B. (2003) Per-Pixel Analysis of Forest Structure: Vegetation Indices, Spectral Mixture Analysis and Canopy Reflectance Modeling. In Remote Sensing of Forest Environments: Concepts and Case Studies; Wulder, M.A., Franklin, S.E., Eds.; Kluwer Academic Publishers: Boston, MA, USA; pp. 209–254.

Bianchini, Edmilson, Pimenta, José A., Santos, Flavio A. M. dos. (2001). Spatial and temporal variation in the canopy cover in a tropical semi-deciduous forest. Brazilian Archives of Biology and Technology, 44(3), 269-276.

Cassidy, L., Southworth, J., Gibbes, C., & Binford, M. (2013). Beyond classifications: Combining continuous and discrete approaches to better understand land-cover change within the lower Mekong River region. Applied Geography, 39, 26-45.

Defibaugh y Chávez, Jason; Tullis, Jason A. (2013). "Deciduous Forest Structure Estimated with LIDAR-Optimized Spectral Remote Sensing." Remote Sens. 5, no. 1: 155-182.

FAO (Food and Agriculture Organization). (2011). State of the World's Forests. Rome: FAO. 164p.

Grace, J. (2004). Understanding and managing the global carbon cycle. Journal of Ecology, 92, 189-202

IPCC (2006). Guidelines for National Greenhouse Gas Inventories. In: H.S. Eggleston, L. Buendia, K. Miwa, T. Ngara & K. Tanabe (Eds.). Japan: National Greenhouse Gas Inventories Programme.

IPCC (2010). Expert Meeting on National Forest GHC Inventories. In: Eggleston, H.S.; Srivastava, N.; Tanabe, K., Baasansuren, J. (Eds.). National Forest GHC Inventories – a Stock Taking. Japan: IGES.

Ministério do Meio Ambiente (2011). Pagamentos por Serviços Ambientais na Mata Atlânica: lições aprendidas e desafios. Fátima Becker Guedes e Susan Ed da Seehusen; Organizadoras. – Brasília: MMA. 272 p. (Série Biodiversidade, 42) ISBN 978-85-7738-157-9.

RESUMO

O mapeamento da estrutura florestal em escala de paisagem nos permite avaliar como as florestas respondem aos impactos da ação humana e a mudanças nas condições ambientais. Neste contexto, a tese tem como objetivo elaborar modelos de estimativa de biomassa acima do solo e fechamento de dossel utilizando imagens de satélite, em diferentes estágios de sucessão de Mata Atlântica localizada em área com complexidade topográfica. Para alcançar este objetivo geral, temos dois objetivos específicos: (1) avaliar o efeito da geomorfologia na modelagem da biomassa florestal e fechamento do dossel; (2) analisar os resultados das estimativas considerando diferentes estágios de sucessão florestal e testar o efeito da radiação solar direta sobre o fechamento do dossel. Primeiro, sumarizamos os mais frequentes temas ecológicos e métodos utilizados na literatura ligados a modelagem de estrutura florestal por meio do sensoriamento remoto. Subsequentemente, utilizamos dados de campo e imagens de satélite (LANDSAT TM e ALOS AVNIR-2) para estimar biomassa e fechamento do dossel. Utilizamos modelo digital de elevação como fonte de informação geomorfológica. Foram encontradas melhores estimativas de biomassa e fechamento do dossel quando integramos as imagens de satélite com uma variável geomorfométrica secundária do relevo (Fator de iluminação), que é baseada no ângulo de incidência da radiação solar sobre faces de morros. O índice “solo/vegetação”, elaborado no presente estudo, apresentou melhores estimativas de fechamento do dossel quando comparado com a performance de diferentes índices de vegetação. A biomassa estimada pelas imagens possibilitou a diferenciação entre diferentes estágios de sucessão florestal.

ABSTRACT

Mapping forest structure in landscape scale enables the evaluation of how forested areas respond to human impact and environmental conditions. In this context, the thesis aims to evaluate modeling approaches to estimate forest aboveground biomass and canopy closure with satellite images in different successional forest stands located at a rugged terrain region. Towards that goal, the specific objectives are: (1) to evaluate the effect of topographic features in the remotely sensed biomass and canopy closures estimations; (2) to analyze the modeled data over different successional stands of Atlantic Rainforest and test the effect of the annual direct sunlight in the forest canopy closure. First, we summarize the most frequent ecological inferences discussed in the literature and the methods used about forest structure modeling by using remote sensing data. Afterward, ground biophysical forest data and satellite images (LANDSAT TM and ALOS AVNIR-2) were used to estimate biomass and canopy closure. The modeling approach includes topographic features derived from digital elevation model. Our results show improved biomass and canopy closure estimates when the modeling includes satellite data interacting with a secondary geomorphometric variable (the Illumination Factor), that is based on direct solar beam angle. The soil/vegetation index, suggested in the present study, showed a better performance when compared with other vegetation index to estimate canopy closure. The modeled biomass shows evident biophysical distinction among different forest succession stages.